INVESTIGATION OF THE ATMOSPHERIC CONTINUUM RADIATION USING AIRBORNE MICROWAVE DATA NEAR 600 GHZ AND COMPARISON WITH MODELS

A Thesis Presented
by
Leila Kaviani

to
The Graduate School for the Degree of
Master of Science in Physics

Bremen University.
Institute of Environmental Physics.
February 2003

Devoted to my family.

Contents

List of Figures

Introduction

Remote sensing techniques provide a useful tool for the investigation of the stratospheric chemistry and chemical reactions associated with the depletion of the ozone layer in the upper atmosphere.

The continuum absorption of radiation in the microwave region primarily due to water vapor in the lower troposphere is a problem of great practical as well as theoretical interest. The continuum absorption increases with frequency and the strong absorption by water vapor limits the height for future submillimeter limb sounders.

In the recent years a large number of experimental work and theoretical investigation about continuum and water vapor continuum have been performed. However, most of these studies concentrate on the millimeter and far-infrared regions. The existing continuum models are based on laboratory microwave measurements up to 340 GHz and no validation of continuum models and no comparison between the different continuum models in the submillimeter wave region has been investigated.

The purpose of this work has been to analyze the measurements of the atmospheric continuum radiation primarily due to water vapor using airborne radiometer data and to test existing continuum models in the submillimeter frequency range.

Basic principles of atmospheric sensing, an overview of the physical and chemical properties, the basic concepts of pressure, temperature distributions and composition of the atmosphere are described in chapter 1.

The objectives of chapter 2 are to describe how the submillimeter radiometer ASUR works and to present the basic concepts involved in making radiometric measurements and a presentation of the techniques of three hygrometers.

The chapter 3 introduces the physical basis of microwave absorption by atmospheric molecules and the necessary spectroscopic information. This chapter contains also a short introduction to the field of water vapor continuum, dry air continua and a description of the ARTS forward model.

The microwave data used in this work and the water vapor, temperature and pressure profiles as input to the radiative transfer model to calculate brightness temperatures are demonstrated in chapter 4.

The results of the analysis and the comparison between measurements and calculations including the error analysis are presented in chapter 5.

Chapter 1

Composition and structure of the atmosphere

1.1 Physical properties of the atmosphere

The atmospheric pressure and density decrease approximately exponentially with increasing height, as does the water vapor density and its variation with height is strongly dependent on time of day, season, geographic location, and atmospheric activity.

The Earth's atmosphere can be subdivided into a number of atmospheric layers according to its thermal structure.

As indicated in Figure 1.1, the vertical profile can be divided into four distinct layers: *troposphere*, *stratosphere*, *mesosphere* and *thermosphere*. The layers are separated by the *tropopause*, *stratopause*, and *mesopause*, respectively.

The lowest layer of the Earth's atmosphere is known as the *troposphere* (from Greek tropo [turning, changing]). Here the temperature decreases with increasing altitude, at a rate of about 6.5 K km^{-1}. The *tropopause* varies in height according to latitude, season and weather activity, it is between 8 and 10 km in arctic regions and between 16 and 18 km in the tropical and equatorial regions.

The next layer above the troposphere is the *stratosphere*. The stratosphere extends to a height of about 50 kilometres. In the lower 10 km of the stratosphere the temperature is approximately constant, and it increases with height between 20 and 32 km with a gradient of 1 K km^{-1}, followed by a faster rate of 2.8 K km^{-1} between 32 km and 47 km due to the ozone layer. Above the *stratopause*, the temperature begins to decrease again because the ozone concentration is so low that the heating by solar ultraviolet radiation

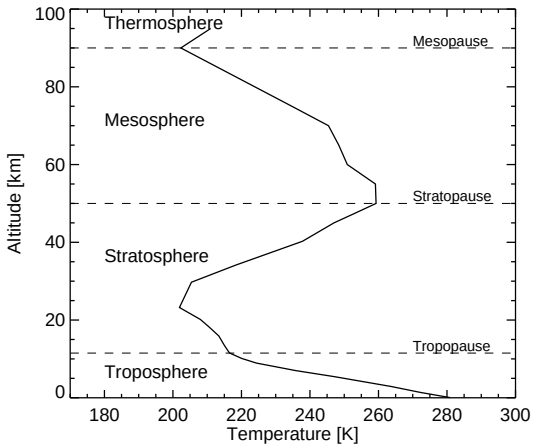

Figure 1.1: Vertical temperature profile of the atmosphere in the polar region. From *National Centre for Environmental predictions (NCEP).*

begins to drop off. This region, extending between the stratopause and approximately 80 to 90 km is the *mesosphere.* In this layer, the temperature decreases to the lowest value of the atmospheric temperature profile. The mesosphere is capped by the *thermosphere.* The thermosphere extends upward to an altitude as several hundred kilometres, where temperature range from 500 K to as much as 2000 K, depending on solar activity.

1.2 Atmospheric composition

The principle constituents of the atmosphere are molecular nitrogen N_2 (78.08%) and molecular oxygen O_2 (20.94 %), and a small contribution of noble gases. Thus about 99 procent of the air is composed of N_2 and O_2. The above gases may be characterized as *constant* gases. In contrast to the constant gases, there are *variable* gases, so called *trace gases* such as H_2O, O_3, CO_2, CH_4, H_2, N_2O, CO and CF_2Cl_2.

The concentration of water vapor and ozone are highly variable in space and time, both gases play extremely important roles in the atmospheric energy balance and in the absorption of the radiation.

1.3 Vertical profiles of pressure

The vertical variability of pressure is much larger than the horizontal and temporal variability of these quantities. The pressure decreases exponentially with height (z)

$$p(z) = p_0 \cdot \exp\left(-\frac{z}{H}\right) \tag{1.1}$$

where $p_0 = 1013.25hPa$ is the reference pressure and H is the *pressure scale height.*

$$H = \frac{R^* \cdot T}{M \cdot g} \tag{1.2}$$

of the order of 7 km, and can be calculated from R^* the universal gas constant for ideal gas, g the gravitational acceleration, M is the molecular weight of air, and T the temperature in Kelvin.

Chapter 2

The instruments

Sub-millimeter sensors represent an important development in the field of remote sensing. These are capable of measuring stratospheric temperature distributions and molecular concentration profiles.

2.1 The ASUR instrument

The **ASUR** (**A**irborne **SU**bmillmeter **R**adiometer) is an aircraft sensor working in the frequency range between 604.3 and 662.3 GHz (wavelengths between 0.45 and 0.5 mm). It detects thermal emission from rotational lines of stratospheric constituents such as ClO, HCl, O_3, N_2O, HNO_3, CH_3Cl, H_2O, HO_2, BrO, $HOCl$, HCN and NO.

The pressure broadening of the detected emission lines provides vertical profiles from 15 to over 50 km altitude, with a vertical resolution of about 6 km and 12 km in the lower and upper stratosphere, respectively. The horizontal resolution is about 12 to 40 km depending on the necessary integration time and the speed of the aircraft.

A major problem in measuring atmospheric sub-millimeter radiation comes from the fact that the atmosphere is not transparent at wavelengths smaller than 0.7 mm (larger than 300 GHz). This absorption is mainly due to water vapor, most of which is found in the troposphere and hence can only be avoided by measuring above the water vapor i.e at an altitude of 10-12 km (tropopause) .

In winter 1991/1992 [Crewell 1993] [5], the instrument **SUMAS** [1] (earlier version of ASUR) participated in the first European Arctic Stratospheric Ozone Experiment (EASOE). It was operated on board the German Aerospace Research facilities (DLR) research aircraft 'Falcon'.

[1] **SU**b **m**illmeter **A**tmospheric **S**ounder

Since then the sensor took part in almost every national and international winter campaign, such as during the SESAME campaign (Second European Stratospheric Arctic and Mid-latitude Experiment) in 1994/1995 where the Schottky-diode detector was replaced by a liquid-helium cooled **S**uperconductor- **I**nsulator- **S**uperconductor (SIS) diode mixer.

In winter 1999/2000, the ASUR instrument participated in the THESEO-2000 /SOLVE campaign. Measurements were carried out in the Arctic high-latitude region on board the NASA DC-8 research aircraft.

Since the first flight, the ASUR instrument has been continuously improved, and the frequency range has been extended to measure new species. The system noise temperature has been reduced, which corresponds to the reduction of the integration time obtaining the same sensitivity, and hence increases the spatial and temporal resolution.

2.1.1 The Setup of the ASUR instrument

The ASUR instrument is a passive heterodyne radiometer working in the frequency range of 604.3-662.3 GHz.

In Figure 2.1 a schematic view of the ASUR instrument is shown. The ASUR structure is divided in two parts, the so-called *front-end* and the *back-end*.

2.1.2 The Front-end

The atmospheric signal enters the aircraft at an elevation angle of 12° (zenith angle of 78°) through a HDPE (High Density Polyethylene) window which is nearly transparent at sub-millimeter wavelengths. The first element in the front-end is a turnable mirror, and the mirror position is controlled by a stepper motor, which compensates the aircraft roll angle. This ensures that all atmospheric measurements are performed at the same elevation angle. The rotatable plane mirror also switches between the atmospheric signal and two black bodies at liquid nitrogen and at ambient temperature for the purpose of calibration.

The atmospheric signal and the *local oscillator* signal are coupled into the mixer by so-called *quasi-optical* components. The mirror reflects the atmospheric or calibration signal into the quasi-optical system.A description of the quasi-optics is shown in Figure 2.2. The quasi-optical system contains the *temperature calibration*, a *path length modulator*, and two *Martin-Puplett* interferometers.

One of the Martin-Puplett interferometers is used as a single *side band* filter, to suppress the unwanted side band. The other is used as a *diplexer*

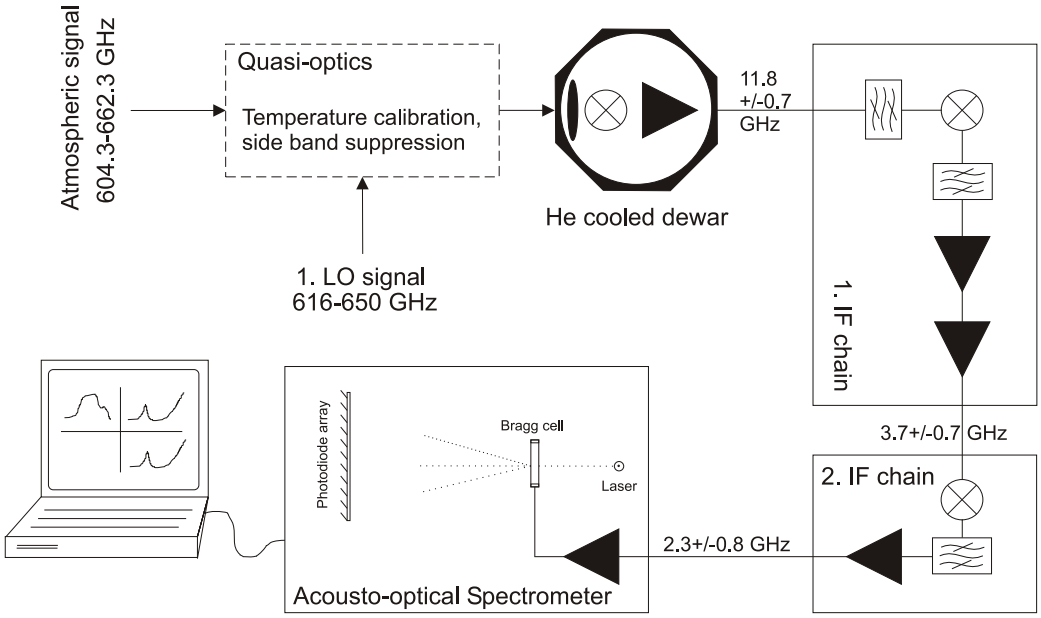

Figure 2.1: Schematic overview of the ASUR instrument: *quasi-optics*, *liquid helium-cooled SIS Diode mixer*, *1. and 2. intermediate frequency chain*, and *Acousto-Optical Spectrometer* (AOS).

to combine the atmospheric and the local oscillator signal and injects them into the mixer.

A *Path length modulator* is used to reduce standing waves between the mixer and the calibration unit or the atmospheric window. However, the Path length modulator usually has been turned off during the flights since no standing waves occurred.

The local oscillator signal (LO) with a fixed frequency is heterodyned with the atmospheric signal. Finally the signal is focused into the antenna of the mixer. The detector is a superconducting [2] diode (SIS-diode), that is located inside the dewar and cooled to liquid helium temperature at 4.2-2.7 K depending on the ambient pressure.

The received atmospheric radiation is mixed with the fixed frequency

[2]In general thermal noise of a detector is produced by the random motions of electrons and atoms. This effect can be reduced by lowering the temperature of the detector. Therefore superconducting devices, which work at low temperature will show very low noise temperature.

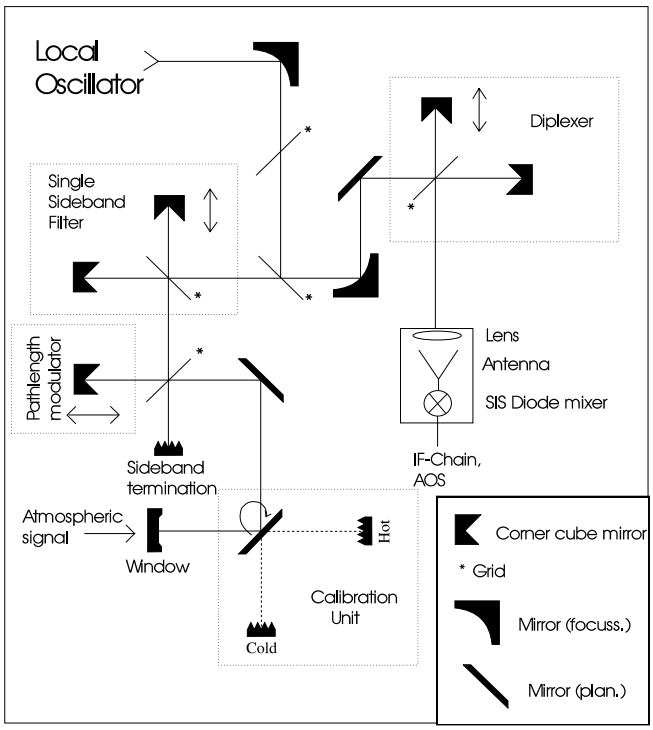

Figure 2.2: The ASUR *quasi-optics* with a calibration unit, Pathlength modulator, single-side-band (SSB) filter, Diplexer and SIS Diode.

of the local oscillator between 616.8 and 649.8 GHz to generate the first *intermediate frequency band* with a centre frequency of 11.4 GHz (heterodyne mixing process). The LO frequency is provided by a *Gunn oscillator* which is controlled by a *Phase lock loop* (PLL) using a 100 MHz reference. The down converted signal is amplified and filtered by band pass filters.

The first amplifier is a high quality low noise amplifier [HEMT] cooled to liquid nitrogen to guarantee a low system noise temperature of the radiometer. After the second amplifier the signal is again converted to 3.7 GHz which is the input frequency of the back-end.

2.1.3 The Back-end

The back-end consists of an intermediate frequency (3.IF) chain, a computer system and an *acousto-optical spectrometer*. After the third intermediate frequency chain the signal is further converted down to the input frequency of the AOS (2.3 ± 0.8 GHz).In the back-end, the down converted signal is amplified, filtered and spectrally analysed.

The acousto-optical spectrometer (AOS) is used for the frequency analysis of the observed band. The AOS consists of a temperature stabilised laser which illuminates a *Bragg cell*. This crystal is excited acoustically by the down converted 2.3 GHz IF signal and the light is diffracted by the travelling waves in the cell. Thus the transmitted laser beam is deflected by the density variations in the crystal generated by the acoustic wave, and then detected by a CCD array.

The AOS spectrometer is employing 1728 channels. Each channel has a width of 0.89 MHz, the usable total bandwidth is 1.3 GHz at an effective resolution of 1.5 MHz.

2.2 Heterodyne principle

In a heterodyne receiver the received signal (*the radio-frequency* or RF signal) is translated to a lower frequency (*the intermediate-frequency* or IF signal), where low noise amplifiers are available.

The RF signal is combined with a fixed frequency signal, which is generated by a local oscillator (LO), using a nonlinear element (SIS-Diode) which produces the intermediate frequency.

The advantage of this type of detection is that the complete information of the RF signal (i.e. spectral shape and intensity) remains unchanged, only the frequency band is transformed to a lower frequency band. Thus it is possible to amplify and filter and analyse the band using electronical components.

The heterodyne principle can be formulated in terms of the frequencies :

$$\nu_{IF} = |\nu_{LO} - \nu_{RF}| \tag{2.1}$$

It can be seen that two bands are transformed to the IF band : the upper (usb), respectively the lower side band (lsb).

$$\nu_{lsb} = \nu_{LO} - \nu_{IF}, \quad \nu_{usb} = \nu_{LO} + \nu_{IF} \tag{2.2}$$

Therefore, to suppress the unwanted side band an SSB Filter can be applied.

2.3 Calibration procedure

Any receiving system produces noise output. The noise power of a heterodyne receiver is composed of the noise power of the detected signal by the antenna and the noise power of the receiver components:

$$P = P_{ant} + P_{sys} \tag{2.3}$$

Making use of the *Nyquist* theory and assuming the validity of the *Rayleigh-Jeans* approach, which results in a proportionality between radiated power and temperature for a black body, in other words between the noise power and the noise temperature :

$$P = k_B \cdot T \cdot \Delta\nu \tag{2.4}$$

where k_B the Boltzmann constant and $\Delta\nu$ the band width in Hz. P is the noise power and T the noise temperature.

Therefore we can write

$$T = T_{ant} + T_{sys} \tag{2.5}$$

Since it is not possible to distinguish between the two noise terms T_{ant} and T_{sys} , specific calibration techniques are used to separate the signal T_{ant} from the receiver noise.

The receiver power is expressed as an equivalent brightness temperature, the physical temperature of an ideal black body to generate the same radiation as observed. If we assume local thermodynamic equilibrium, the Planck function is given by

$$B_\nu(T) = \frac{2h\nu^3}{c^2} \frac{1}{\exp(\frac{h\nu}{k_B T}) - 1} \tag{2.6}$$

where T is physical temperature in Kelvin, $h = 6.62 \cdot 10^{-34}$ J s is Planck's constant, ν is frequency in Hz, $k_B = 1.38 \cdot 10^{-23}$ J K^{-1} is Boltzmann's constant, $c = 2.9979 \cdot 10^8$ m s^{-1} is the speed of light.

The calibration of the instrument is done by observing the radiation from black bodies with a known temperature (77 K and ambient temperature). The calibration method is the *total-power* measuring principle, where the radiometer is calibrated by measuring the atmospheric signal and compare it with the measurements of hot and cold (P_{hot} and P_{cold}) calibration loads.

The atmospheric temperature T_A can be calculated by

$$T_A = T_{cold} + (P - P_{cold}) \cdot \frac{T_{hot} - T_{cold}}{P_{hot} - P_{cold}} \tag{2.7}$$

The system noise temperature T_{sys} can be measured by the *Y-factor* method, where the Y-factor is defined as :

$$Y = \frac{P_{sys}^{hot}}{P_{sys}^{cold}} \tag{2.8}$$

where P_{sys}^{hot} and P_{sys}^{cold} are the power at the hot and cold temperatures, respectively.

The output power of the receiver during calibration is due to the noise power of the complete receiver system, which can be expressed as the system noise temperature T_{sys}

$$T_{sys} = \frac{T_{ant}^{hot} - Y \cdot T_{ant}^{cold}}{Y - 1} \tag{2.9}$$

where T_{hot} and T_{cold} are the physical radiating temperatures of the hot and cold loads respectively.

The sensitivity of an ideal radiometer is given by the radiometer formula

$$\Delta T_A = \frac{K \cdot T_{sys}}{\sqrt{\Delta\nu \cdot \tau}} \tag{2.10}$$

Where ΔT_A is the minimum detectable signal, T_{sys} the system noise temperature, τ integration time, $\Delta\nu$ the frequency width, the factor K is a constant, which is determined by the type of receiver. For a *total-power* receiver is $K = 1$ [Bremer H.] [1].

2.4 Window transmission

The atmospheric signal enters the aircraft through a HDPE window, which has good transmission at sub-millimeter frequencies. The window usually consists of a dielectric material with two parallel surfaces, which induces internal reflections, resulting in a fabry-perot etalon effect. Hence the window used in the Falcon for ASUR observation is slightly wedged to suppress interferences between the window surfaces.

The influence (emission, absorption and reflection) of the window on the measured signal must be known a priori because it is not included in the calibration procedure.

In the Rayleigh-Jeans approximation, the observed intensity is expressed in terms of the observed temperature T_{obs} and the sky signal in terms of the sky temperature T_{sky}:

$$T_{obs} = T_{sky} \cdot t + T_{in} \cdot r + T_{win}(1 - r - t) \tag{2.11}$$

where the T_{in} is the temperature inside the aircraft, T_{win} is the window temperature, t is the transmittance and r the reflectance of the window.

The contribution of the window to the observed signal can be calculated considering the known window transmission and reflection as well as the measured window temperature and inside-air temperature of the aircraft.

$$T_{corr} = \frac{1}{t} \cdot \Big(T_{obs} - (1 - t - r) \cdot T_{win} - r \cdot T_{in} \Big) \tag{2.12}$$

2.5 The other instruments

Water vapor is an invisible gas that is present everywhere in the atmosphere. The distribution of atmospheric water vapor is of fundamental importance to weather and climate, atmospheric radiation and atmospheric chemistry. Three basic humidity measurement techniques commonly used for airborne and ground-based atmospheric research are: the thermoelectrically cooled chilled-mirror dew-point hygrometer (dew/frost point temperature), the Lyman α hygrometer (absolute humidity) and Polymer capacitance sensor (relative humidity).

There are many active earth and satellite based research programmes for water vapor studies. The National Oceanic And Atmospheric organisation (NOAA), and NASA operate DC-8, and ER-2 research aircraft and balloon platforms which provide measurements of water vapor in the upper troposphere and stratosphere.

Water vapor levels drop from around 13,000 ppmv at ground level to about 5 ppmv at high altitudes. However, there is often disagreement among measurements of water vapor performed by different techniques, even from the same platform. The following instruments were participated on the NASA DC-8 during THESEO 2000/SOLVE to measure water vapor mixing ratio.

2.5.1 Tunable Diode Laser (TDL) Spectrometer

Water vapor volume mixing ratio is measured using second harmonic absorption spectroscopy at 1.37 μm wavelength. A single frequency Tunable Diode Laser (TDL) is used for the measurement. A tunable diode laser system is able to provide high accuracy measurements of gases active in the infrared spectrum, namely water vapor (H_2O), carbon dioxide (CO_2), carbon monoxide (CO), acetylene (C_2H_2), ammonia (NH_3), oxygen (O_2), hydrogen chloride (HCl) and others.

JPL open-path tunable diode laser spectrometer

Two near-infrared aircraft instruments have been developed at the Jet Propulsion Laboratory (JPL) [May, 1998] and have been flown on the NASA ER-2 and DC-8 research aircraft. Both operate with similar electronics and software but differ in their external optical arrangements.

For the DC-8 instrument, which in this case measures tropospheric water vapor, an optical path length of 50 cm was chosen. In this case a multipass system is not needed and the laser beam travels a simple "there and

back" path between the laser/detector head, and small return mirror. With this system measurements from about 30000 to 8 ppmv can be made. The analyses of the spectra generates a quantifiable gas concentration in real time.

Number density is the basic quantity measured by the laser hygrometer, and can be converted to volume mixing ratio, dew point, etc using measurements of pressure and temperature.

This non-contact technique has good long-term stability and high accuracy. It's simplicity and ease of maintenance makes it a very good candidate for use in process applications. It is a basic measurement monitoring the gas itself rather than measuring an effect on the surface of a sensor.

This spectrometer has been used to measure water vapor profiles which served as input parameters for the forward calculation.

Accuracy: +5% (limited by accuracy of calibration standards)
Precision: 1-2% at 5 ppmv water vapor, 1 s response time
Response Time: 0.128s minimum, 1s typically

LaRC/ARC diode laser hygrometer (DLH)

The Diode Laser Hygrometer (DLH) was developed by NASA's Langley and Ames Research Centres (LaRC and ARC) and has been flown on the DC-8 aircraft.

The sensor consists of a compact laser transceiver mounted to a DC-8 engine enclosure to complete the optical path. Using differential absorption detection techniques gas-phase water H_2O is sensed along this 28.5 m external path. The H_2O measurement is unaffected by clouds, haze, etc and thereby enabling high spatial resolution measurements in and around clouds.

This sensor has a number of advantages including compactness, simple installion, fast response time, no wall effects, and wide dynamic measurement range.

Precision: 2% or 0.2 ppmv
Response Time: 50 msec

2.5.2 Tropospheric Ozone and Tracers from Commercial Aircraft Platforms (TOTCAP)

TOTCAP was designed to fly for long durations on commercial aircraft to measure several trace gases. TOTCAP was initially deployed on NASA's DC-8 flying laboratory during the SOLVE campaign to study ozone loss in

the northern hemisphere. Measurements of ozone (by ultraviolet absorption), water vapor (by near-infrared tunable diode laser spectroscopy), carbon dioxide (by near-infrared absorption), and halocarbon (by gas chromatography) are performed continously during the aircraft flight, every second for O_3, H_2O and CO_2 and every four minutes for halocarbon. Water vapor is detected with a tunable diode laser spectrometer (designed by Randy May) and this sensor has an internal absorption path, optimised for the mid-troposphere.

Precision:	1-2%
Detection Limit:	10 ppm
Response Time:	1 sec

Chapter 3

Microwave radiation transfer

3.1 Radiative transfer equation

The radiative transfer equation is the fundamental equation describing propagation of electromagnetic radiation in a scattering and absorbing medium. It is ideally suited for radiative transfer in media such as the atmosphere.

The interaction between radiation and matter is described by two processes, namely: *extinction* and *emission*.

If radiation traversing in a medium is reduced in intensity, we have *extinction*, and if the medium adds energy of its own, we have emission. The energy lost from the incident radiation may have been absorbed by the material, scattered, or both. By absorption loss, the energy is transformed into other forms of energy, such as heat. By scattering loss, the energy caused to travel in direction other than the direction of the incident radiation.

The *extinction coefficient* can be expressed as the sum of an absorption coefficient and a scattering coefficient. At microwave frequencies scattering by air molecules can be normally neglected, because the wavelengths (0.1-1 mm) are considerably larger than air molecules.

We have only to consider absorption and emission. Therefore, the radiative equation can be written as

$$\frac{dI_\nu}{ds} = -\alpha_\nu I_\nu + S_\nu \tag{3.1}$$

Where I_ν is the specific intensity, which is defined as the flux of energy in a given direction per second per unit frequency interval per unit solid angle per unit area, ν the frequency, s the distance along the propagation path, α the absorption coefficient, and S the source term.

In the absence of scattering and under the assumption of *local thermal equilibrium*[1] the *Kirchoff's law* states that the specific intensity emitted and absorbed are equal. The source function is the absorption coefficient times the *Planck function*

$$S_\nu = \alpha_\nu B_\nu(T) \tag{3.2}$$

Where the Planck function B is defined as :

$$B_\nu(T) = \frac{2h\nu^3}{c^2}\frac{1}{e^{h\nu/kT}-1} \tag{3.3}$$

Here, h is the Planck's constant, k is the Boltzmann's constant, c is the speed of light and T is temperature in Kelvin.

For the conditions given, no scattering and local thermodynamic equilibrium, the radiative transfer equation can be solved analytically, yielding *the integral form of the radiative transfer equation*

$$I_\nu = I_0 e^{-\tau_\nu(h,\infty)} + \int_h^\infty \alpha_\nu B_\nu(T) e^{-\tau_\nu(h,s)} ds \tag{3.4}$$

Where τ is the *optical depth* defined as:

$$\tau(s,s') = \int_s^{s'} \alpha_\nu(s') ds' \tag{3.5}$$

Where I_0 is the background radiation depending on the observation geometry, h is the distance along the path to the limit of the media.

3.1.1 Brightness temperature

The brightness temperature is defined as the temperature of a black body, that produces the same intensity magnitude as observed.

The brightness temperature is calculated as

$$T_b = \frac{h\nu}{k_B}\frac{1}{\ln\left(\frac{2h\nu^3}{c^2 I_\nu}+1\right)} \tag{3.6}$$

Where I_ν is the specific intensity.

[1]For the frequency considered and altitudes below about 75 km, the absorption and emission coefficients will be equal.

For lower frequencies $h\nu/(k_B T) \ll 1$ [2] the Planck function can be approximated by the *Rayleigh-Jeans* law.

$$B(\nu, T) = \frac{2\nu^2 k_B T}{c^2} = \frac{2k_B T}{\lambda^2} \tag{3.8}$$

The Rayleigh-Jeans approximation can be used to frequencies up to 300 GHz.

The Rayleigh-Jeans approximation of the Planck function gives a *natural definition of brightness temperature*:

$$T_{rj} = \frac{c^2}{2\nu^2 k_B} \cdot I_\nu \tag{3.9}$$

The important aspect of equation (3.9) is the linear relationship between the intensity and the brightness temperature. The difference between the physical temperature and brightness temperature increase with frequency.

Though the Rayleigh-Jeans approximation is not valid in the submillimeter wavelength range, the measured intensity is normally indicated as brightness temperature in unit Kelvin.

---

[2] $$\exp\Big(\frac{h\nu}{k_B T}\Big) \approx 1 + \frac{h\nu}{k_B T} \tag{3.7}$$

Gas absorption

In general there are three types of absorption/emission spectra:

Resonant lines, non-resonant absorption of dry atmosphere due to collision-induced mechanisms involving electric quadrupole, and continuum like water vapor opacity.

3.2 Line absorption

Radiation is absorbed (or emitted) by a molecule when a transition takes place from a lower (or higher) energy state to a higher (or lower) energy state. *Electronic* energy results from the transfer of electrons between different orbits. *Vibrational* energy is associated with vibrational motions of the atoms about their equilibrium positions. *Rotational* energy is associated with rotational motion of the atoms of the molecule about the molecule's centre of mass. For radiation in the microwave region, propagating through a gas, the relevant transitions are rotational transitions of gas molecules. Each transition is visible in frequency dependence of the *absorption coefficient* as a spectral line.

The absorption coefficient α can be written as:

$$\alpha(\nu) = nS(T)F(\nu) \tag{3.10}$$

Where n is the number density of the absorber, $S(T)$ is the *line intensity*, the shape and the position are expressed by the *line shape function* $F(\nu)$.

The total absorption coefficient is given by summing the absorption of all spectral lines of all species.

3.2.1 Line intensity

The line intensity can be expressed as

$$S_{ij}(T) = \frac{8\pi^3 \nu_{ij} \mu_{ij}^2}{3hc} \frac{1}{Q(T)} \left(e^{-\frac{E_j}{k_B T}} - e^{-\frac{E_i}{k_B T}} \right) g_j \tag{3.11}$$

in which a *Maxwell-Boltzmann* distribution of state occupation probabilities has been used. μ_{ij} is the reduced matrix element between levels i and j of the molecular dipole moment, g_j is the statistical weight and $Q(T)$ is the *partition function.*

Partition function

The partition function describes the energy states distribution of the gas particles. The partition function for a perfect gas molecule can be expressed as:

$$Q = Q_{tr} \cdot Q_{int} \tag{3.12}$$

Where Q_{tr} is the *translational partition* function, which accounts for the distribution of the translational energy of the gas particles. Q_{int} is the *internal partition* function, which describes the internal energy distribution of the gas particles between electronic, rotational, vibrational and nuclear spin states.

$$Q_{int} = Q_{el} \cdot Q_{rot} \cdot Q_{vib} \cdot Q_{nuc} \tag{3.13}$$

3.2.2 Line broadening

Each frequency line of the absorption (or emission) spectrum of a molecule corresponds to the transition between quantized energy levels of the molecule. At conditions found in the atmosphere, spectral lines have a width greater than their natural line width. The increase in line width is called *line broadening*. Line broadening results mainly from three factors: *the finite life time of an exited state, pressure-induced collision* and *thermal motion*. The first one is completely negligible under conditions found in the atmosphere.

Doppler (thermal) broadening

Doppler broadening is important for the upper stratosphere and mesosphere at microwave frequencies. The thermal motion of the molecules produces a Doppler shift of the emitted radiation. At thermal equilibrium the velocity of the atmospheric molecules has a *Gaussian distribution*. The line shape can be described by the Doppler function:

$$f_{Doppler}(\nu) = \frac{1}{\gamma_D \sqrt{\pi}} \cdot \exp\left(-(\frac{\nu - \nu_0}{\gamma_D})^2\right) \tag{3.14}$$

Where the Doppler line width γ_D is given by

$$\gamma_D = \frac{\nu_0}{c}\sqrt{\frac{2RT}{M}} \tag{3.15}$$

R is the universal gas constant and M is the molecular weight.

Pressure broadening

Pressure broadening is the most important mechanism for atmospheric absorption in the microwave region of the spectrum. Pressure broadening is a result of collisions between molecules. These collisions shorten the life time of the states involved in the transition and the corresponding line will be broadened.

The largest part of the broadening is caused by nitrogen and oxygen molecules, denoted as *air broadening*. The broadening caused by other molecules of the same species is called *self broadening*.

The pressure broadening is more complicated than Doppler broadening. Therefore various approximation can be used. The most popular approximation is the *impact approximations*, which states that the duration of the collisions is short compared to the average time between collision. This leads to the *Lorentz line shape*:

$$F_{Lorentz}(\nu) = \frac{1}{\pi}\frac{\gamma_L}{(\nu - \nu_0)^2 + \gamma_L^2} \tag{3.16}$$

Where γ_L is the Lorentz line width. The temperature and pressure dependence of the width is calculated as

$$\gamma_L = \gamma_0 \frac{p}{p_0}\left(\frac{T}{T_0}\right)^n \tag{3.17}$$

i which p is the pressure , γ_0 is the line width at the reference temperature p_0 and the reference temperature T_0 and n is the exponent for the temperature dependency (between zero and one).

A correction to the Lorentz line shape for the microwave region is the *Van Vleck-Weisskopf line shape*

$$F_{VWW}(\nu) = \left(\frac{\nu}{\nu_0}\right)^2 \frac{\gamma_l}{\pi}\left(\frac{1}{(\nu-\nu_0)^2+\gamma_L^2} + \frac{1}{(\nu+\nu_0)^2+\gamma_L^2}\right) \tag{3.18}$$

In the middle atmosphere and at frequencies above 100 GHz the difference [3] between the Lorentz and the Van Vleck-Weisskopf is negligible [Eriksson 1999] [6].

Voigt line shape

In the upper stratosphere and mesosphere, where both Doppler and pressure broadening are significant, both effects have to be included. The line shape function has to be approximated in this case by the *Voigt* line shape function.

$$F_{Voigt}(\nu,\nu_0) = \int_{-\infty}^{\infty} F_{Lorentz}(\nu,\nu')F_{Doppler}(\nu',\nu_0)d\nu' \tag{3.19}$$

This integral cannot be solved analytically, some kind of numerical approximation is needed.

[3] Differences between the Lorentz and Van Vleck-Weisskopf line shape occur in the line centre and in the far wings of the line

3.3 Atmospheric continua

Measurements in both pure water vapor and moist air show much higher values than expected theoretically by model calculations of pure resonant line absorption predicted by using a standard Van Vleck-Weisskopf (VVW) line shape function. This difference is usually called *continuum* or *non resonant* absorption.

Continuum absorption in the earth's atmosphere can be divided into two categories: *water vapor continuum*, which depends quadratically on water vapor partial pressure, and *dry air continua* (non resonant absorption by O_2 and collision induced absorption by N_2 and CO_2), which depend only on temperature and total pressure.

In the troposphere water vapor is the dominant source [4] of continuum absorption. In the stratosphere, frequency regions sufficiently far away from water vapor spectral lines, dry air continua are dominant [Buehler 1999] [2].

3.3.1 Water vapor continuum

Water vapor plays a fundamental role in the energy balance of the earth. It is not only the most important absorber of out-going thermal radiation (greenhouse gas), but is responsible for about 70% of the atmospheric absorption of in-coming solar radiation.

The non resonant absorption can be caused by a perturbation of the molecule wave function during *collision* or it may be the result of *far wings* from the infrared region, in addition *water Dimers*, $(H_2O)_2$ can have also an influence.

Since the pioneering measurements of *Beck and Autler [1946]*, it has been known that the absorption by water vapor is not completely attributable to nearby spectral lines. Various models therefore include *semi-empirical* corrective terms to represent far wing behaviour of absorption which is called the "*continuum*", in addition to line contributions.

These models, which are generally developed for the infrared, have been applied to various microwave regions. In principle the distinction between local-line and continuum absorption is arbitrary, because only the total absorption can be measured. The continuum is what remains after subtraction of line contributions and the latter depend on the number of lines considered, on the intensities, and on the shape, which may or may not have a cutoff at far wing frequencies.

[4] under extreme conditions such as in the Antarctic winter, dry air continua can play an important role even in the troposphere.

Other laboratory measurements of water vapor absorption have been made by *Frankel and Woods [1966], Liebe [1984], .Liebe 1993 [9].Liebe and Layton [1987], Godon et al.[1992] and Bauer et al.[1993,1995,1996].*

Ma and Tipping [1990] [10] give a theoretical treatment of continuum absorption by pure water vapor, in which the absorption is due to the collision-broadened far wings of the numerous submillimeter and far-infrared resonances.

A statistical treatment based on the approximation was proposed by *Rosenkranz.* *Clough et al.* proposed a theoretical line shape based on a modified impact approximation. *Thomas and Nordstrom* submitted a line shape based on different models for the line centre , near wing or far wing regions, and involving many empirical parameters.

All these theories were not able to reproduce the observed absorption and its temperature dependence in all the spectral regions. Then a semi-empirical model was developed by Clough et al. (CKD), and a large number of experimental works has been produced by the groups led by H.Liebe and A.Bauer.

Model calculation

The continuum absorption coefficient α_c, is generally defined as the difference of the total absorption coefficient α_{tot}, and the resonant line absorption coefficient α_l

$$\alpha_c = \alpha_{tot} - \alpha_l \tag{3.20}$$

The resonant line absorption coefficient (α_l) depends on the different spectral line catalogs and the selected line shape.

The continuum part can be separated into two components

$$\alpha_c = \alpha_{c,s} + \alpha_{c,f} \tag{3.21}$$

Where $\alpha_{c,s}$ *self broadening* [5] is due to interaction of two water molecules, and $\alpha_{c,f}$ *foreign broadening* [6] describes the far wing absorption of water vapor due to collisions between water molecules and nitrogen molecules.

$\alpha_{c,s}$ is proportional to the square of water vapor partial pressure (P_{H_2O})

$\alpha_{c,s} \quad \propto \quad P^2_{H_2O}$

[5] self broadening means the enlargement of line width due to interactions with molecules of the same species

[6] foreign broadening means the enlargement of line width due to interactions with molecules of different species

while $\alpha_{c,f}$ is proportional to the product of water vapor pressure (P_{H_2O}) and dry partial pressure

$\alpha_{c,f} \quad \propto \quad P_{H_2O} \cdot P_d$

$$P_d = P_{tot} - P_{H_2O} \tag{3.22}$$

$\alpha_{c,s}$ has a much stronger temperature dependence than $\alpha_{c,f}$

The Liebe model

The **M**illimeter wave **P**ropagation **M**odel (MPM) is presented to predict propagation effects of loss and delay for the non precipitating atmosphere up to 1000 GHz and for temperatures ranging from $-100°C$ to $+50°C$ but the altitude coverage is only up to 30 km. Contributions from dry air, water vapor, suspended water droplets (haze, fog, cloud) and rain are addressed.

The MPM consist of 44 O_2 and 30 H_2O for the '89 version (MPM89) and 34 H_2O for the '93 version (MPM93) local line spectra (below 1000 GHz), non resonant spectra for dry air and an empirical water vapor term, which describes experimental discrepancies with observed absorption.

A line-by-line summation of spectra by the two principle absorber molecules, O_2 and H_2O accounts to the resonance absorption.

The model that Liebe used up to '89 version is called *simple empirical model*. In the version of '93, Liebe employed one *pseudo-line parameterisation*. An analytical match of the continuum was considered by means of a *pseudo-line* centred at about 1780 GHz. This pseudo-line can be accounted to balance all the missing lines above 1 THz [7]. Frequencies above 500 GHz, the discrepancies between pseudo-line parameterisation (MPM93) and simple empirical model (MPM89) become significant large.

Water vapor line spectrum: The total line absorption α_l of water vapor is the sum over all individual lines:

$$\alpha_l = N_{H_2O} \sum_k (S_k(T) F(\nu, \nu_k)) \tag{3.23}$$

With N_{H_2O} the number density, $S_k(T)$ the individual line strength and $F(\nu, \nu_k)$ the line shape function.

The line data base consists of six parameters for each line. Two parameters, b_1 and b_2 describe the line strength and its temperature dependence

$$S_k(T) = \frac{b_1}{\nu_0} P_{H_2O} \Theta^{3.5} e^{b_2(1-\Theta)} \tag{3.24}$$

[7] The most important water vapor lines are below 1THz

Where ν_0 is the line centre frequency, P_{H_2O} is the water vapor partial pressure and Θ is defined as

$$\Theta = \frac{300K}{T} \tag{3.25}$$

The other four parameters describe the Lorentz line width γ_i

$$\gamma_i = b_3(b_4 P_{H_2O}\Theta^{b_6} + P_d\Theta^{b_5}) \tag{3.26}$$

Where P_d is the partial pressure of dry air.

The Liebe 87, 89 and 93 use an original Van Vleck-Weisskopf (VVW) line shape function.

Water vapor continuum spectrum: The continuum absorption of water vapor is calculated as:

$$\alpha_c = \nu^2 \cdot P_{H_2O} \cdot (C_s \cdot P_{H_2O} \cdot \Theta^{X_s} + C_f \cdot P_d \cdot \Theta^{X_f}) \tag{3.27}$$

C_s, X_s, C_f, X_f are the self broadening and foreign broadening parameters, respectively. X_s, X_f are two temperature dependent parameters.

The c_s is much larger than c_f and the temperature dependence of the these four constant parameters are different for MPM87 and MPM89. In the MPM93 which Liebe added one pseudo-line, which it makes quite complicate in respect to older versions.

The Clough-Kneizys-Davies model

The Clough-Kneizys-Davies Model (CKD) is a water vapor continuum model, which is based on a water vapor monomer line shape formalism applied to all spectral regions from the microwave to the infrared. The revisions that have been made to the CKD model improved selected spectral regions of the model's self and foreign broadened water vapor continua but did not modify its basic formalism.

The CKD model is a *true line-by-line* far wing model, describes the water vapor continuum as an extra effect of the far wings of the H_2O spectral lines.

The CKD line shape function F_{CKD} can be divided into two parts:

$$F_{CKD}(\bar{\nu}, \bar{\nu}_i) = F^l_{CKD}(\bar{\nu}, \bar{\nu}_i) + F^c_{CKD}(\bar{\nu}, \bar{\nu}_i) \tag{3.28}$$

With the terms

$$F^l_{CKD}(\bar{\nu}, \bar{\nu}_i) = f_l(\bar{\nu} - \bar{\nu}_i)\chi(\bar{\nu} - \bar{\nu}_i) + f_l(\bar{\nu} + \bar{\nu}_i)\chi(\bar{\nu} + \bar{\nu}_i) \tag{3.29}$$

and

$$F^c_{CKD}(\bar{\nu},\bar{\nu}_i) = f_c(\bar{\nu}-\bar{\nu}_i)\chi(\bar{\nu}-\bar{\nu}_i) + f_c(\bar{\nu}+\bar{\nu}_i)\chi(\bar{\nu}+\bar{\nu}_i) \tag{3.30}$$

With F^l_{CKD} as the line shape function produces the line spectrum and F^c_{CKD} as the line shape function produces the water vapor continuum.

The χ function is a *semi-empirical function* applied to the impact result to correct for duration of collision effects [8] and to provide agreement between calculated and measured spectra. With $\chi = 1$ the line shape reduces to the Lorentz shape in the infrared and to the Van Vleck-Weisskopf shape in the microwave.

f_l is defined as the Lorentz function:

$$f_l(\bar{\nu},\pm\bar{\nu}_i) = \begin{cases} \frac{1}{\pi}\{\frac{\gamma_i}{(\bar{\nu}\pm\bar{\nu}_i)^2+\gamma_i^2} - \frac{\gamma_i}{\bar{\nu}^2_{cutoff}+\gamma_i^2}\} & \text{if } \mid \bar{\nu}\pm\bar{\nu}_i \mid \leq \bar{\nu}_{cutoff}, \\ 0 & \text{if } \mid \bar{\nu}\pm\bar{\nu}_i \mid > \bar{\nu}_{cutoff}, \end{cases} \tag{3.31}$$

With the cutoff wavenumber $\bar{\nu}_{cutoff} = 25\ cm^{-1}$. The cutoff avoids applying the line shape to distant frequencies and also establishes a limit to the summation in Eq 3.23.

The CKD model defines a continuum line shape by removing the line centre from the Lorentz line shape function:

$$f_c(\bar{\nu},\pm\bar{\nu}_i) = \begin{cases} \frac{1}{\pi}\frac{\gamma_i}{\bar{\nu}^2_{cutoff}+\gamma_i^2} & \text{if } \mid \bar{\nu}\pm\bar{\nu}_i \mid \leq \bar{\nu}_{cutoff}, \\ \frac{1}{\pi}\frac{\gamma_i}{(\bar{\nu}\pm\bar{\nu}_i)^2+\gamma_i^2} & \text{if } \mid \bar{\nu}\pm\bar{\nu}_i \mid > \bar{\nu}_{cutoff}, \end{cases} \tag{3.32}$$

The self and foreign continuum coefficients $\tilde{C}_s$ and $\tilde{C}_f$ are defined as:

$$\tilde{C}_{s,f} = \sum_i \tilde{S}_i(T)[f(\bar{\nu}-\bar{\nu}_i)\chi_{s,f}(\bar{\nu}-\bar{\nu}_i) + f(\bar{\nu}+\bar{\nu}_i)\chi_{s,f}(\bar{\nu}+\bar{\nu}_i)] \tag{3.33}$$

The pressure dependence is the same as that of the simple empirical model. The water vapor continuum absorption coefficient is given as:

$$\alpha(\bar{\nu}) = \bar{\nu}^2\frac{hc}{2KT_0}\frac{n_0}{p_0^2}\left(\frac{T_0}{T}\right)^3 P_{H_2O}[\tilde{C}_s(T)P_{H_2O} + \tilde{C}_f(T)P_d] \tag{3.34}$$

Where n_0 is the number density at the reference temperature $T_0 = 296\ K$ and $p_0 = 1013.25\ hPa$.

[8] collision effects are neglected by using pure Lorentz or Van Vleck-Weisskopf line shape functions.

The temperature dependence of the foreign broadened continuum is the same as in the MPM89 model. The self continuum for water vapor demonstrates a rather strong temperature dependence as T^{-3} and it as not possible to compare directly because C_s itself has also temperature dependence. This is a disadvantage of the CKD continuum model.

The different versions of the CKD model use the same set of self and foreign continuum coefficients and improve them with a *correction function* which depends only on the wave number.

The Rosenkranz model

The water vapor continuum formulation of Rosenkranz is a recommended model for atmospheric radiative transfer calculations. Rosenkranz is a reinvestigation of Liebes [1987] millimeter-wave propagation model (MPM) for the foreign broadened component of the water vapor continuum and of the 1993 version of MPM for the self broadened component and of CKD-2.1 [Buehler 2000] [3].

The local line absorption is calculated as

$$\alpha_l = N_{H_2O} \sum_i S_i(T)[f_i(\nu) + f_i(-\nu)] \tag{3.35}$$

N_{H_2O} is the number density of water molecules, ν is the frequency, and the line intensities $S(T)$, which are functions of temperature T, are calculated from the HITRAN database and 15 lines with a frequency lower than $1THz$ are considered.

The line shape $f_i(\nu)$ has a cutoff at $\nu_{cutoff} = 750\ GHz$ and subtracted baseline as given by CKD model but do not include the semi-empirical correction function χ.

$$f_i(\nu) = \begin{cases} \left(\frac{\nu}{\nu_i}\right)^2 \frac{1}{\pi}\left\{\frac{\gamma_i}{(\nu \pm \nu_i)^2 \pm \gamma_i^2} - \frac{\gamma_i}{\nu_{cutoff}^2 + \gamma_i^2}\right\} & \text{if } \mid \nu \pm \nu_i \mid \leq \nu_{cutoff}, \\ 0 & \text{if } \mid \nu \pm \nu_i \mid > \nu_{cutoff}, \end{cases} \tag{3.36}$$

Where ν_i is the line centre frequency and γ_i is the line half width, which is calculated as

$$\gamma_i = w_s \cdot P_{H_2O} \cdot \Theta^{X_s} + w_f \cdot P_d \cdot \Theta^{X_f} \tag{3.37}$$

Where w_s, X_s, w_f and X_f are constant coefficients and P_{H_2O} is the partial pressure of water vapor and P_d is the partial pressure of dry air components. These constant coefficients differ only in minor respects from the values used by Liebe 89.

If $\nu_{cutoff} \rightarrow \infty$ Eq. (3.35) and Eq. (3.36) combined would be equivalent to a Van Vleck-Weisskopf line shape.

The Rosenkranz formulation of the water vapor continuum assumed the structure from the MPM87 model:

$$\alpha_c = \alpha_{c,s} + \alpha_{c,f} = \nu^2 \cdot \Theta^3 \cdot (C_s \cdot P_{H_2O}^2 + C_f \cdot Pd \cdot P_{H_2O}) \tag{3.38}$$

It is also well known that the frequency dependence of the microwave spectrum of any molecule is that as the Fourier-transformed autocorrelation function of the dipole moment responsible for the absorption multiplied by the square of frequency. The product ΘP_{H_2O} is proportional to gas density.

The self and foreign continuum coefficients C_s and C_f respectively can be calculated as:

$$C_s = 7.80 \cdot 10^{-6} \cdot \Theta^{4.5} \qquad (\frac{dB}{km})/(GHz^2 \cdot kPa^2) \tag{3.39}$$

and

$$C_f = 2.36 \cdot 10^{-7} \qquad (\frac{dB}{km})/(GHz^2 \cdot kPa^2) \tag{3.40}$$

The values for C_s and C_f have been increased by 3% and 15% respectively in respect to the original values of MPM93 (for self broadened continuum) and MPM87 (for foreign broadened continuum), which use an original Van Vleck-Weisskopf line shape function without cutoff and base subtraction.

3.3.2 Dry air continua

Dry air continua are caused by three different molecules namely nitrogen(N_2), oxygen (O_2) and carbon dioxide (CO_2).

The oxygen molecule has no permanent electrical dipole moment but has a permanent magnetic dipole moment resulting from the fact that two of the orbital electrons are unpaired. The two lowest spectral lines also relevant for microwave regions occur at 60 GHz and 118.75 GHz. However, contribution of oxygen continuum is neglected for submillimeter frequencies.

Nitrogen and carbon dioxide have no permanent dipole moments, therefore isolated molecules of these gases do not exhibit pure rotational spectra. However these molecules have electric quadrupole moments. During collisions, the quadrupole moment of one molecule interacts with the polarizability of its partner to induce a dipole moment in the partner molecule [Rosenkranz-98] [12].

The carbon dioxide continuum can be neglected in the earth's atmosphere in the frequency range from 16 GHz to 3.5 THz.

Non-resonant oxygen absorption

The microwave absorption spectrum of oxygen consists of a large number of absorption lines spread out over the 50-70 GHz frequency range (known as the 60 GHz oxygen complex) and an additional line at 118.75 GHz, which is defined as *the spin-rotational spectrum.* In contrast to the spin-rotational spectrum, *the pure rotional spectrum* begins with a line at 368 GHz and extends up to 6 THz. The non-resonant absorption is part of the spin-rotational spectrum.

Liebe model is the most used absorption model for the oxygen absorption.

The total absorption (α_{tot}) can be divided into a spectral line (α_l) and a continuum term (α_c) (like for water vapor):

$$\alpha_{tot} = \alpha_l + \alpha_c \tag{3.41}$$

Rosenkranz (PWR 93) oxygen absorption model

Resonant oxygen absorption : The oxygen line catalog has 40 lines (33 lines around 60 GHz). The line absorption is expressed by

$$\alpha_l^{R98} = \frac{n_{H_2O}}{\pi} \sum_{k}^{40} S_k(T) F(\nu, \nu_K) \tag{3.42}$$

With the number density of O_2

$$n_{O_2} = \frac{0.20946 \cdot P_{air}}{k_B \cdot T} \tag{3.43}$$

Each line strength can be calculated as

$$S_k(T) = \frac{S_k(300K)}{exp(b_k \cdot \Theta)} \tag{3.44}$$

where $S_k(300K)$ describes the reference line intensity at $T = 300K$ and the exponential term assumes the approximation to the exact partition function.

The Van Vleck-Weisskopf function was modified by Rosenkranz to include line overlap effects with the line width:

$$\gamma_k = w(P_d \cdot \Theta^{0.8} + 1.1 \cdot P_{H_2O}) \tag{3.45}$$

where P_{H_2O} is the partial pressure of water vapor and P_d is the partial pressure of the other atmospheric constituents.

For oxygen, their temperature and pressure dependence can be modelled by the sum of two terms

$$Y = P_{air} \cdot \Theta^{0.8} \cdot [\gamma_k + (\Theta - 1) \cdot \nu_k] \tag{3.46}$$

Oxygen continuum absorption : The standard theory for non-resonant absorption is the *Debye Theory.* The Debye line shape is obtained from the Van Vleck-Weisskopf line shape if $\nu_i \to 0$.

The Rosenkranz model also uses the Debye theory for the oxygen continuum absorption model

$$\alpha_c = C \cdot P_d \cdot \Theta^2 \cdot \frac{\nu^2 \cdot \gamma_c}{\nu^2 + \gamma_c^2} \tag{3.47}$$

Where γ_c is the line width.

Liebe (MPM 93) oxygen absorption model

Oxygen line absorption : The oxygen line catalog consists of 44 lines (37 lines around 60 GHz). The oxygen line absorption can be described by

$$\alpha_l^{MPM} = 0.1820 \cdot \nu^2 \cdot \sum_k^{44} S_k(T) F(\nu, \nu_K) \tag{3.48}$$

The line intensity is determined by

$$S_k(T) = \frac{a_{1,k}}{\nu_k} \cdot P_d \cdot \Theta^3 \cdot exp[a_{2,k} \cdot (1 - \Theta)] \tag{3.49}$$

The Van Vleck-Weisskopf line shape function can be used with the line width γ_k and overlap δ_k parameters

$$\gamma_c = a_{3,k} \cdot 10^{-3} \cdot (P_d \cdot \Theta^{a_{4,k}} + 1.1 \cdot P_{H_2O} \cdot \Theta) \tag{3.50}$$

and

$$\delta_k = P_{air} \cdot \Theta^{0.8} \cdot [a_{5,k} + \Theta \cdot a_{6,k}] \tag{3.51}$$

The coefficients a_1, a_2, a_3, a_4, a_5 were established as the best fit to laboratory measurements at 60 GHz absorption by dry air. The oxygen absorption in the wings of the oxygen lines is much higher than in the Rosenkranz model because Liebe model sets only the positive contributions of the line spectrum.

Oxygen continuum absorption : Liebe et al.[1993] also used the Debye theory for their model(like Rosenkranz) and the only difference is the formulation of the line width:

$$\alpha_c = C \cdot P_d \cdot \Theta^2 \cdot \frac{\nu^2 \cdot \gamma_c}{\nu^2 + \gamma_c^2} \tag{3.52}$$

$$\gamma_c = w \cdot P_{tot} \cdot \Theta^{0.8} \tag{3.53}$$

Nitrogen continuum absorption

Nitrogen has neither electric nor magnetic dipole moment (but an electric quadrupole moment), hence it does not have a rotational spectrum. The electric field of the quadrupole moment of one molecule induces a dipole moment in the second molecule and these collision induced absorption by nitrogen can be considered to the dry air continua.

Rosenkranz [1993] [11] and Liebe et al. [1993] are available models for nitrogen absorption in the frequency range below 1000 GHz. The simplest model is given by Rosenkranz [1993]. Rosenkranz [1993] uses an empirical expression similar to the simple empirical term for water vapor. The absorption coefficient, which is given by the sum of all induced dipole absorption lines can be calculated as:

$$\alpha_c = C \cdot \nu^2 \cdot \Theta^{3.5} \cdot P_{N_2}^2 \tag{3.54}$$

With $C = 4.56 \cdot 10^{-13} \frac{dB}{(KmhPa^2GHz^2)}$

The MPM models have only an additional frequency dependent term compared to Rosenkranz model:

$$\alpha_c = \hat{C} \cdot (1.0 - 1.2 \cdot 10^{-5} \cdot \nu^{1.5}) \cdot \nu^2 \cdot \Theta^{3.5} \cdot P_{N_2}^2 \qquad : MPM89 \tag{3.55}$$

$$\alpha_c = \hat{C} \cdot \frac{\nu^2}{(1.0 + a \cdot \nu^{n_{1.5}})} \cdot \Theta^{3.5} \cdot P_{N_2}^2 \qquad : MPM93 \tag{3.56}$$

Where the parameter is $\hat{C} = 2.55 \cdot 10^{-13} \frac{dB}{(KmhPa^2GHz^2)}$ and $a = 1.9 \cdot 10^{-5} GHz^{-1.5}$.

3.4 ARTS

The *forward model* [9] **ARTS**[10] is a tool for the calculation of microwave radiative transfer equation in the millimeter and sub-millimeter spectral range. The ARTS model has been developed to simulate ground based, nadir looking, limb-sounding, balloon/aircraft measurements.

The programs consists of different modules, for example, calculation of absorption coefficients, monochromatic pencil-beam radiative transfer and antenna convolution.

In this work ARTS has been applied to compute the absorption coefficients and calculate the brightness temperatures. There are two ways to calculate the absorption coefficients in ARTS. The first one calculates the cross section x per molecule, the second one calculates the absorption coefficients α from the cross sections and the volume mixing ratios VMR at altitude i defined as

$$\alpha_i = x_i \times VMR_i \tag{3.57}$$

3.4.1 Complete water vapor models

In ARTS several complete water vapor absorption models are implemented and can be easily applied. These models are the MPM87, MPM89, MPM93, CP98 and PWR98. The three MPM and PWR98 can be used for fast absorption calculation in the frequency range of 1-1000 GHz.

The line shape used for α_l and the formulation of α_c make the main difference between the different models.

MPM87/89: Water vapor line catalog consists of 30 lines from 22 GHz upto 998 GHz . The line shape function is the standard Van Vleck-Weisskopf (VVW) function. A set of six parameters $(b_1, b_2, b_3, b_4, b_5, b_6)$ per line described the line absorption (two for the line strength and four for the line width) from [arts] [4].

MPM93: Water vapor line catalog consists of 34 lines below 1000 GHz (four more than in MPM87/89). The line shape function is the same as MPM87/89. MPM93 was formulated in terms of a pseudo-line. The parameters of the water vapor continuum are $\nu*, b*_1, b*_2, b*_3, b*_4, b*_5, b*_6$.

[9] The radiative transfer program used at IUP (Institute of Environmental Physics at University of Bremen) is called forward model

[10] Atmospheric Radiative Transfer System

CP89: Water vapor line catalog consists of only a single line at $\nu_0 = 22\ GHz$ because CP98 is especially designed to determine the ground based radiometer data in the $20 - 31.4\ GHz$ region. The water vapor line absorption is based on MPM87 and CP98 uses the same water vapor continuum parameterisation as MPM87.

PWR98: Rosenkranz assumed the same principle as MPM89. The Rosenkranz uses the different water vapor line catalogs compared with MPM89. The PWR98 uses the Van Vleck-Weisskopf line shape function with cutoff at 750 GHz.

3.4.2 Complete oxygen models

Liebe (MPM93) and Rosenkranz (PWR93) models are the most used absorption models in ARTS.

3.4.3 Complete nitrogen models

Similar to the oxygen absorption models, Rosenkranz (93) and Liebe (93) are the most absorption models in ARTS.

Chapter 4

Data Analysis and interpretation

4.1 Measurements

During the SOLVE/THESEO 2000 campaign the NASA's DC-8 research aircraft accomplished twenty-three flights in three different deployments (from Nov.30 to Dec.16, 1999, from Jan.14 to Jan.29, 2000, and from Feb.27 to Mar.15, 2000) over Scandinavia, and the Arctic polar region [Kleinboehl 2001] [7]. ASUR measurements were performed during all flights.

The operational base during the flight campaigns was Kiruna airport, Northern Sweden. The mean flight time for each flight was approximately 9 hours. The typical flight altitude of about (10-12km) is well above the arctic tropopause, sufficiently high to avoid the strong absorption by water vapor at submillimeter wavelengths in the lower atmosphere.

The measurement geometry is defined by a zenith angle of 78° and the instrument is observing orthogonally to the flight direction. The antenna beam is symmetric in vertical and horizontal direction, with a beam width of 1.3° (full width at half maximum).

Data from the aircraft internal navigation system are used to keep the observing geometry constant and are stored to locate the accurate position of the measured profiles.

In order to study the continuum absorption, the measurements observed during the descent of the aircraft have been selected. From the available data set, a subset of measurements from three flights has been chosen which have performed during the descent of the aircraft: flight number 11 on January 20, 2000, flight number 18 on March 5, 2000, flight number 22 on March 13, 2000.

Flight number	Date (UT)	Time (UT)	Altitude range (km)
11	20.01.00	17:14	5.5 - 10.3
18	05.03.00	19:50	4.9 - 9.3
22	13.03.00	23:10	6.3 - 11.8

Table 4.1: Overview of three flights performed by the ASUR instrument on board the NASA research aircraft DC-8 during the THESEO 2000/SOLVE campaign.

4.2 Data analysis

The signal emitted by the species under study (for example HCl) needs to be extracted from the measured signals. For this purpose, the measured spectrum is calibrated and corrected for the window transmission. Calibration is accomplished by comparing the atmospheric signal alternately to two blackbodies , one at ambient and one at liquid nitrogen temperature, respectively. An individual calibrated spectrum is obtain every 6-8 seconds.

As example the result for the HCl emission line is shown in Figure 4.1. The HCl line at 625.91 GHz is located on the wing of an ozone line at 625.37 GHz. By suitable choice of the receiver centre frequency it is possible to measure HCl and ozone simultaneously.

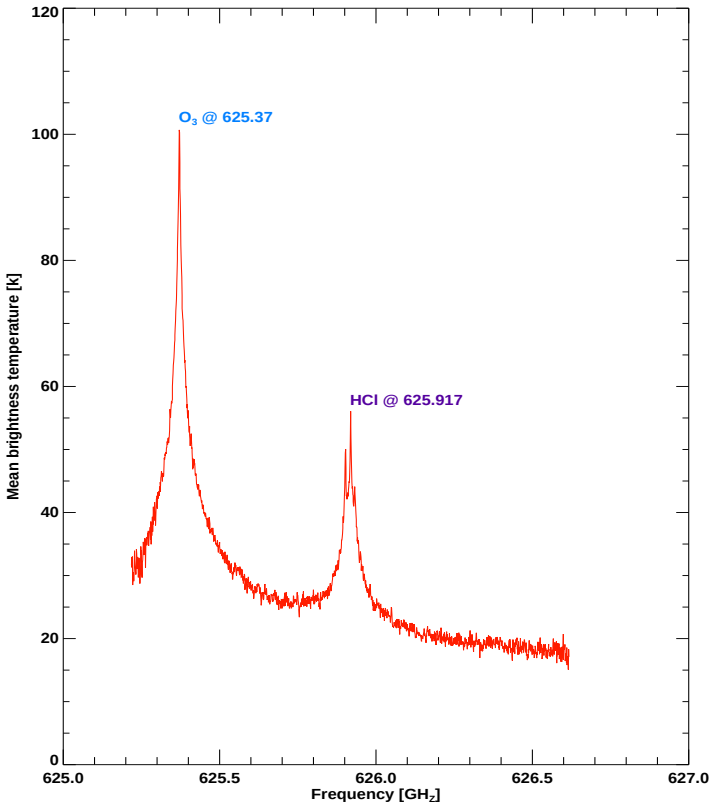

Figure 4.1: Measured HCl / O_3 spectrum by the ASUR sensor.

Rare spectra containing spikes or large baseline distortion are omitted to adulteration of the measurements.

To study the continuum absorption the spectra were averaged over the frequency range between 626.46-626.51 GHz to obtain one brightness temperature for each altitude level. This part of spectrum has been chosen since there is with impact of line contributions.

To ensure that the zenith angle remains constant during the measurements, the actual aircraft roll angle is read in real-time from the on-board computer. This information is used to adjust the angle of the switching mirror relative to the aircraft, before starting the two seconds exposure of every single spectrum. The spectra which have a roll angle larger than 3.5° were excluded in the integration procedure to avoid impact by the window edges.

As can be seen in Figure 4.2 in the flight number 11 (20.01.2000) at altitudes about 7.5-10 km the deviation of the roll angles during the descent of the aircraft are larger than 3.5 degrees and the spectra were not taken, in the flight number 18 (05.03.2000) they are smaller than 2.5 degrees and in the flight number 22 (13.03.2000) smaller than 2 degrees.

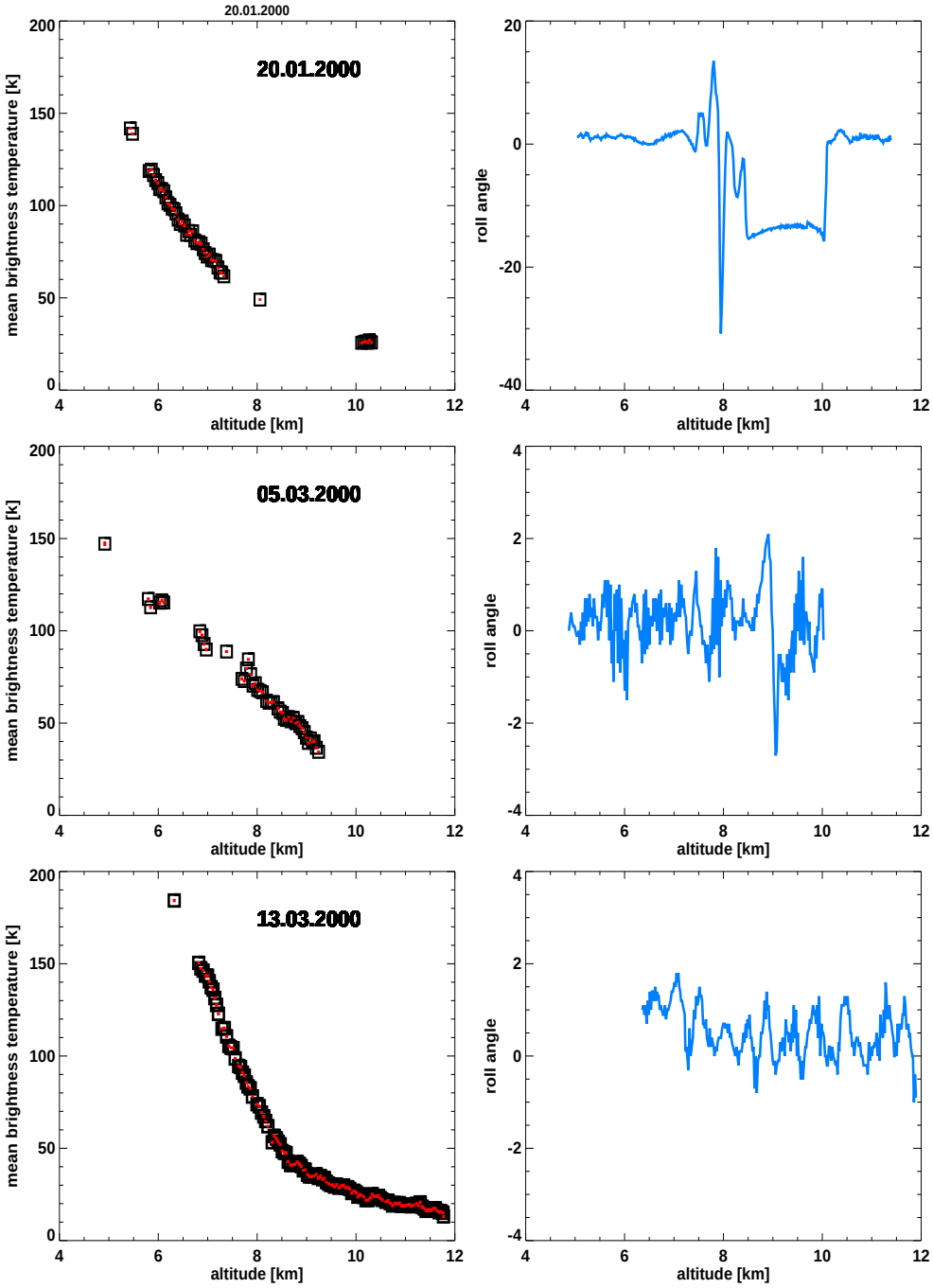

Figure 4.2: The brightness temperature and the roll angle during the descent.

In Figure 4.3, the relative humidity and volume mixing ratio of water vapor against the altitude during the descent of the aircraft for the three flights have been plotted. In flight number 11 (20.01.2000) at altitudes about 5-6.5 km, where the relative humidity is higher than 80 percent, for flight number 18 (05.03.2000) at altitudes about 8-9 km and for flight number 22 (13.03.2000) at altitudes about 6.5-8 km, there is a probability for cloud occurrence during the descent, however this probability is small.

The relative humidity and the volume mixing ratio data have been taken from the Near-Infrared Tunable Diode Laser spectrometer, which has an accuracy about 5%.

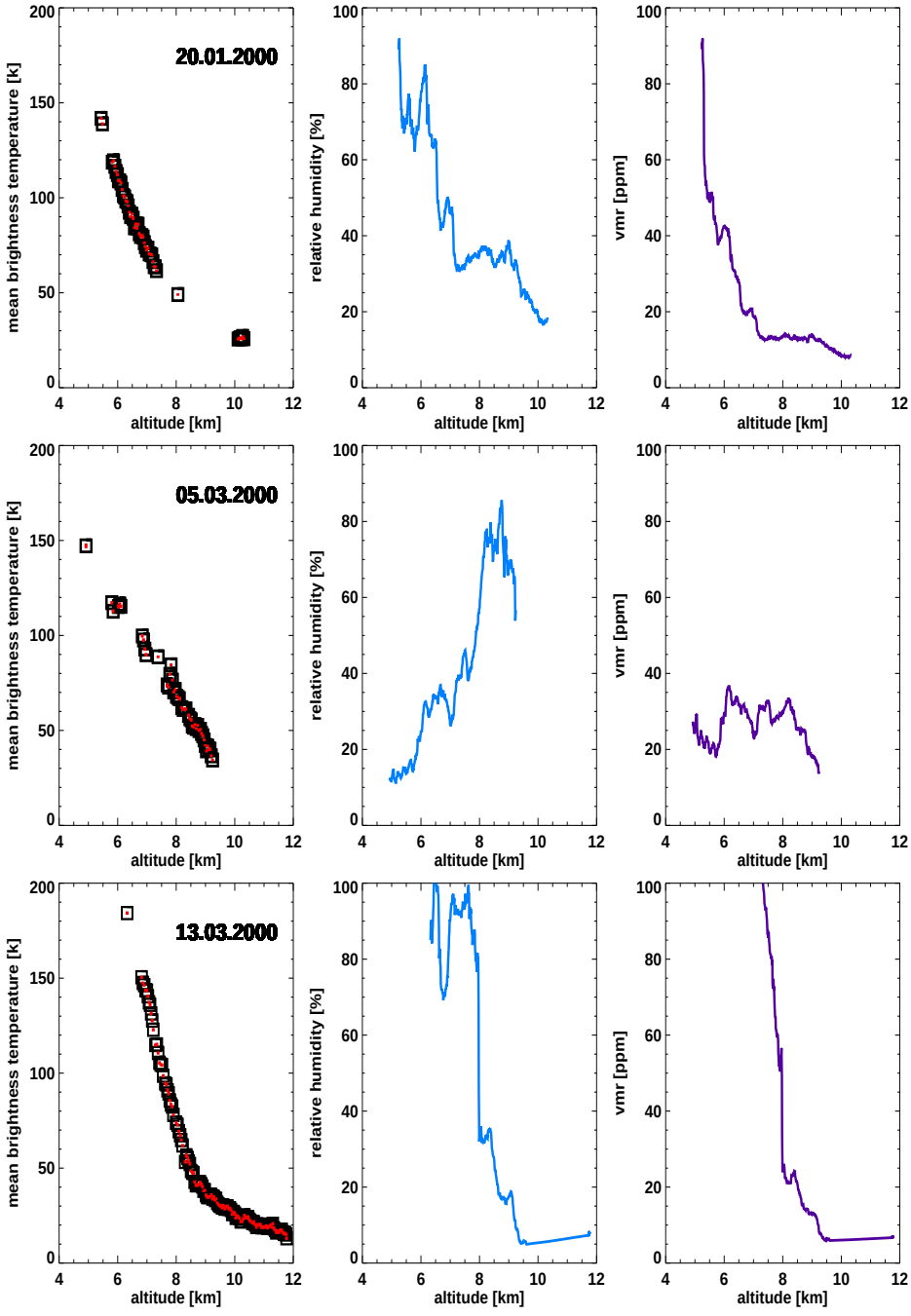

Figure 4.3: The brightness temperatures, relative humidity and volume mixing ratio profiles.

4.3 Calculation of brightness temperature

For the comparison of ASUR measurements with calculated data an accurate and fast radiative transfer model has been used. The computation of absorption coefficients and the radiative transfer calculation have been carried out with the ARTS model for the observing geometry as given for the ASUR.

The radiative transfer model ARTS is a function of additional parameters, so called model parameters e.g. the temperature and pressure profile of the air and the pressure broadening coefficient of the observed emission line.

The required atmospheric data (pressure, temperature, altitude and volume mixing ratio) for use in the ARTS are selected for two altitude ranges:

- From the observed altitude to maximum flight altitude: temperature, pressure and altitude are taken from DC-8 data, volume mixing ratio of water vapor are obtained from the Near-Infrared Tunable Diode Laser spectrometer and volume mixing ratio of HCl and O_3 are taken from FASCOD data.

- above the maximum flight altitude up to 95 km: temperature, pressure and altitude are taken from analyses by the Data Assimilation Office (DAO), and volume mixing ratio profiles of water vapor are obtained from chiou (SAGE II [1] climatology) and the volume mixing ratios of HCl and O_3 are taken from ASUR measurements. These data are the retrieved profiles from the ASUR spectra observed shortly before the descent of the aircraft.

For the calculation, the HCl line at 625.91 GHz is used. In this case the considered line is located on the wing of an ozone line, and the contributions of the N_2 and H_2O continua are also considered in the forward model ARTS.

An example of a calculated HCl/O_3 spectrum is shown in Figure 4.4.

[1] the **S**tratospheric **A**erosol and **G**as **E**xperiment II is a third generation satellite-borne sensor that utilises the solar occultation technique in the visible to near infrared spectral region to measure the concentration of different species in the atmosphere.

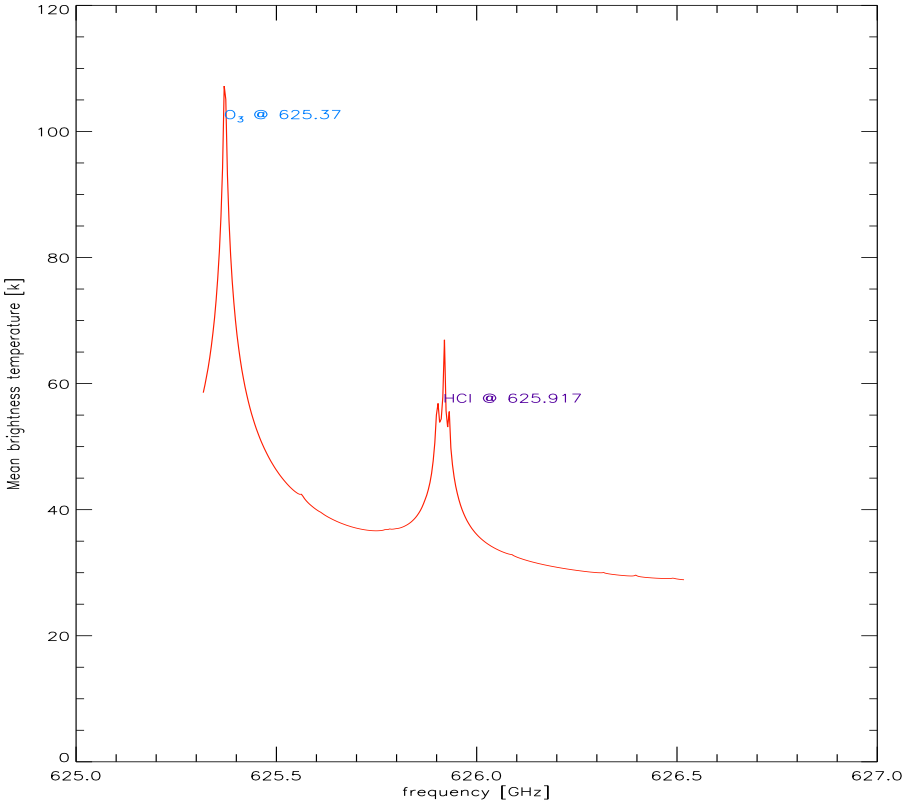

Figure 4.4: The calculated spectrum by the forward model ARTS.

Chapter 5

Results

5.1 Comparisons

Comparisons are done between the observed brightness temperatures and those predicted by the radiative transfer model ARTS. In this study three different water vapor continuum models (PWR 98, MPM93 and MPM89) have been used. The same nitrogen continuum model (MPM 93) has been used with all two water vapor models.

The comparison of the PWR98 and MPM93 water vapor continuum models with ASUR observations for two different flights are shown in Figure 5.1.

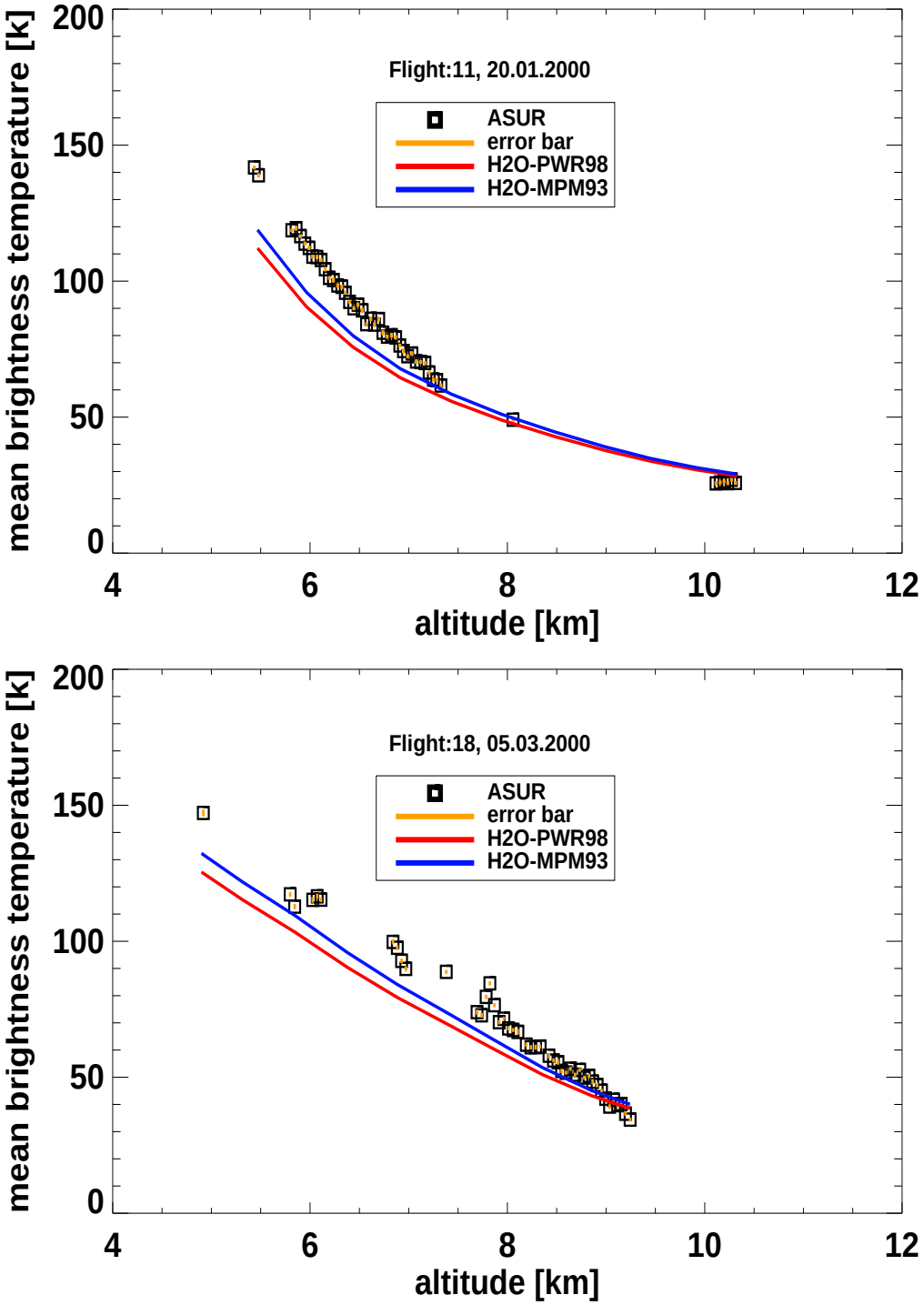

Figure 5.1: The comparison between the measured and the calculated brightness temperature with two different water vapor continuum models for two flights. The error bars are corresponding to the measurement noise

As can be seen in Figure 5.1 below 9 km the models predict significantly less absorption than that observed, where the high water vapor densities give rise to a dominant water vapor continuum signal. Above 9 km the models predict slightly more absorption than that observed and in this altitude range the atmosphere is dry and nitrogen absorption is predicted to dominate.

The major difference between the measurements and calculation is at low altitudes, where the water vapor absorption dominates. The differences are reduced, almost in the altitude range between the 7 and 10 km.

As can be seen in this figure, for the flight number 11 (20.01.2000) at low altitudes of 5.5 km, the difference between measured and calculated brightness temperature is about 22 K and at high altitudes of 10.5 km is about 3 K. For flight number 18 (05.03.2000) at altitudes of 5 km the difference between measured and calculated brightness temperature is about 15 K and at high altitudes of 9.5 km is about 6 K.

Overall the Liebe 93 gives slightly better agreement than the Rosenkranz 98 model but is not predicting enough absorption, where the absorption is seen to be high.

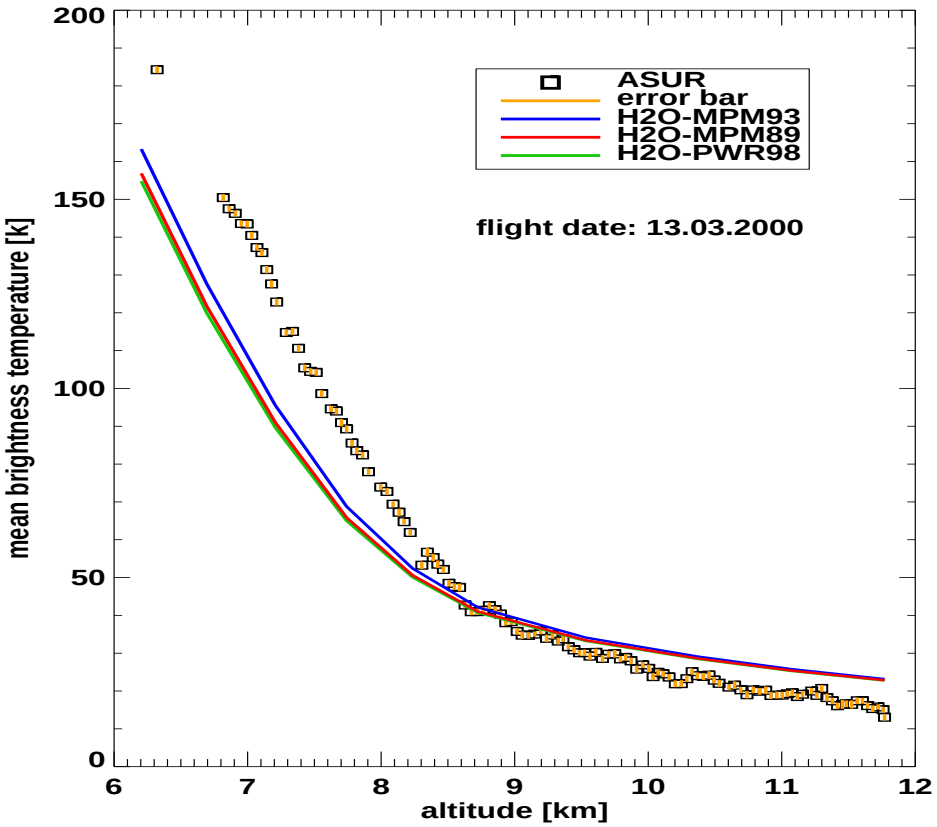

Figure 5.2: The comparison between the measured and the calculated brightness temperature in terms of three different continuum models.

To obtain a more detailed understanding of the performance of the different models, the comparison between the measured and the calculated brightness temperature with three different models (Liebe 93, Liebe 89 and Rosenkranz 98) is shown in Figure 5.2.

The Liebe 93 gives stronger absorption than the other models. The Liebe 89 model gives weaker absorption, but is still greater than the Rosenkranz 98 model. It can be seen in this figure that the Liebe 89 agrees closely with the Rosenkranz 98 because it differs more or less only in the foreign-broadened component.

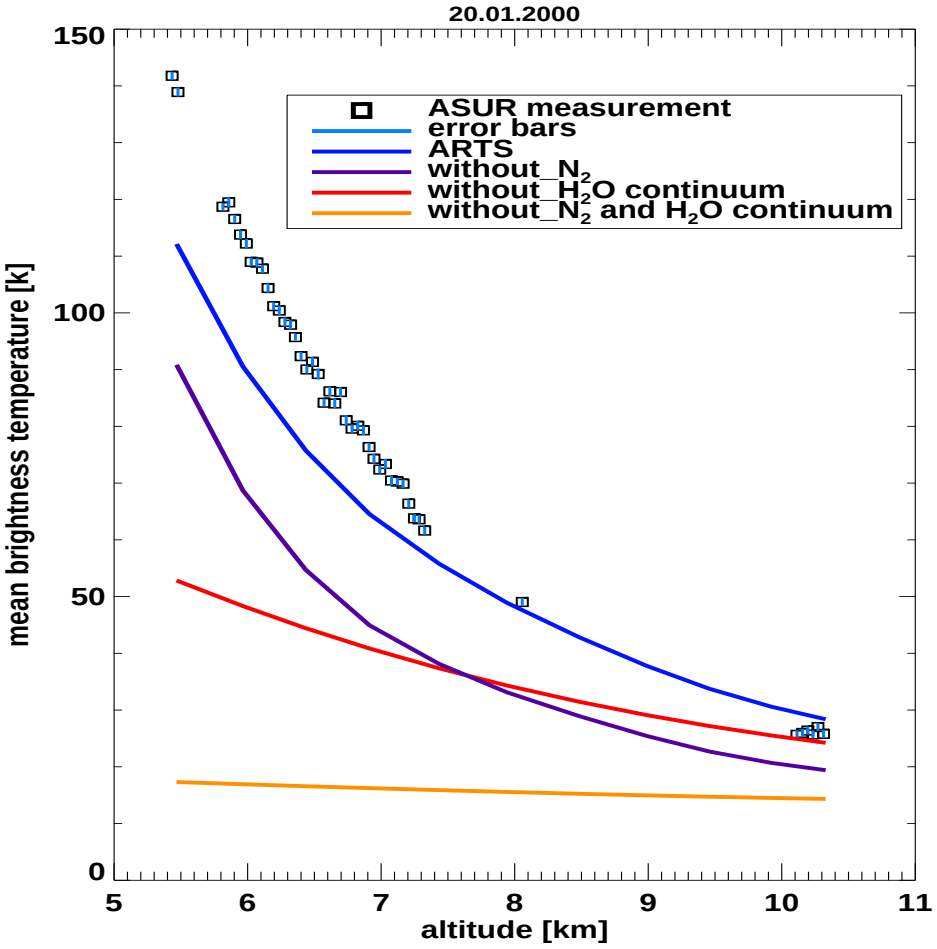

Figure 5.3: The contribution of the water vapor continuum and nitrogen continuum in the calculated brightness temperature.

In Figure 5.3 the water vapor continuum and the nitrogen continuum are compared.

As can be seen in this figure below 8 km the calculation with only water vapor continuum shows more absorption than with only nitrogen continuum and above 8 km the calculation with only nitrogen continuum shows more absorption than with only water vapor continuum.

At low altitudes of 5.5 km the contribution of the water vapor in the total absorption is about 60 K and the nitrogen continuum is about 21 K. At high altitudes 10.5 km the contribution of the water vapor in the total absorption is about 4 K and the nitrogen continuum is about 9 K.

The explanation lies in the fact, that in the troposphere water vapor is the dominant source of continuum absorption and in the stratosphere dry

air continua are dominant that are dominated by collision induced nitrogen absorption.

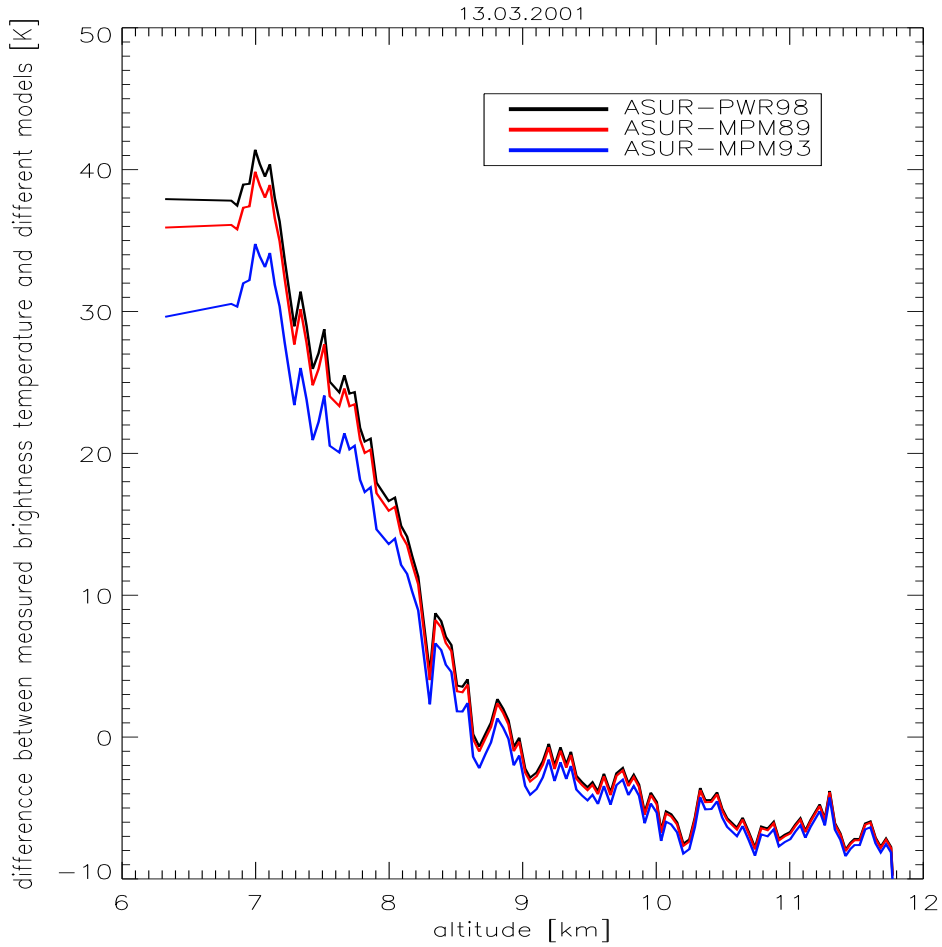

Figure 5.4: The difference between the observed brightness temperature and the three different models (Liebe 93, Liebe 89 and Rosenkranz).

As shown in Figure 5.4 at low altitudes of 6 km the difference between the measured brightness temperature and Liebe 93 is about 30 K, the measured brightness temperature and Liebe 89 is about 36 K and the measured brightness temperature and Rosenkranz 98 is about 38 K. At high altitudes of 11.5 km the differences between the measured brightness temperature and Liebe 93 or Liebe 89 are about 8 K, respectively and the difference between the measured brightness temperature and Rosenkranz 98 is about 7 K. That means at low altitudes, where the water vapor continuum is dominant the difference between three different models is larger than at high altitudes,

where the nitrogen continuum absorption is dominant.

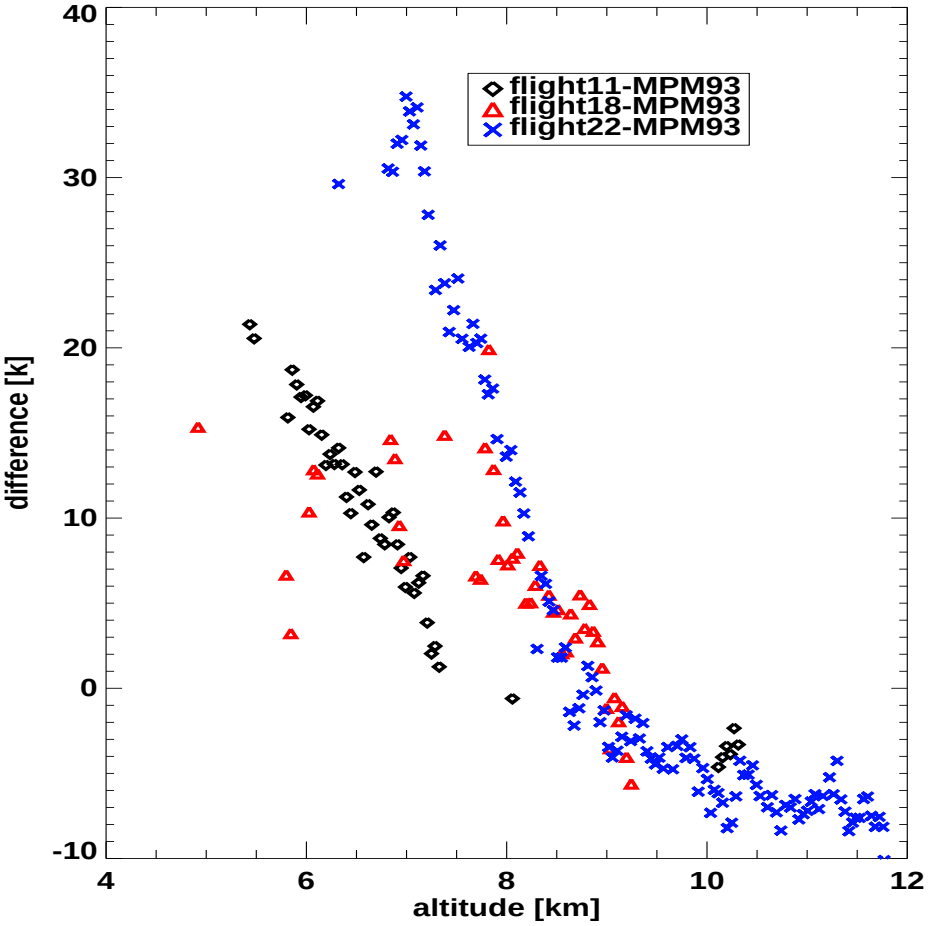

Figure 5.5: The difference between the observed and the calculated brightness temperature for three different flights.

Figure 5.5 shows the difference between calculated and measured brightness temperature for all three flights.

Quantitatively, the three measurements show a similar behaviour, good agreement around 9 km altitude and much stronger absorption below, and still lower absorption above 9 km, compared with the predicted values. However, below 9 km the differences between calculations and measurements vary significantly from flight to flight.

5.2 Error analysis

In the following section an error analysis and an estimation of possible sources of errors have been investigated.

The possible errors identified can be used to estimate the accuracy of the measured and calculated spectra.

5.2.1 Errors in the Measured brightness temperature

The effects which influence the measured spectrum can be separated into two classes:

- statistical errors
- systematic errors

The measurement noise is known as statistical error. Standing waves, cold load reflectivity and pointing accuracy are known as systematic errors.

Measurement noise

The radiometric noise in a total power measurement depends on the receiver system noise temperature, the integration time and the detection band width $\Delta\nu$ as given in Equation(2.10).

The measurement noise can be determined directly from the measurement namely by the standard deviation of the mean value of the brightness temperature. The measurement noise is shown in Figure 5.6.

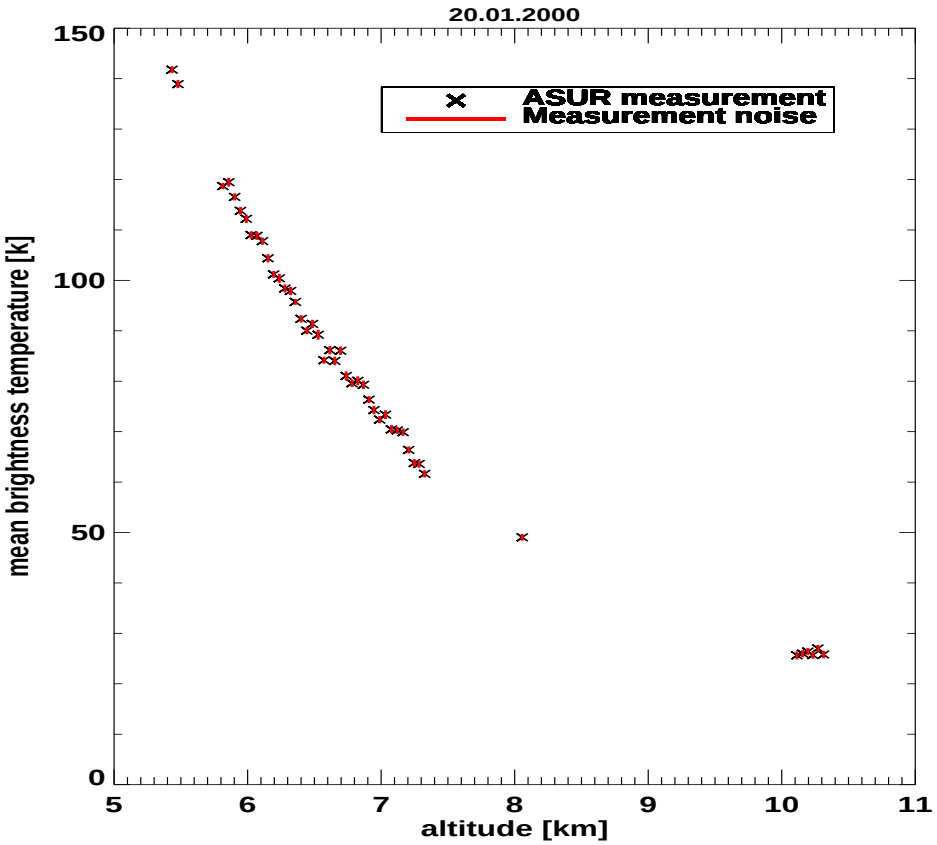

Figure 5.6: The observed brightness temperature by the ASUR sensor and the measurement noise as statical error.

Standing waves

In general, standing waves are caused by reflections on two parallel surfaces, mostly in the quasi-optics, between the window and the calibration loads, by Fabry-Perot interference between the surfaces of the window and in the high frequency cables of the intermediate frequency chain. The standing waves which occur in the quasi-optics can be removed in the calibration sequence when they are persistent. The standing waves which originate from the window and calibration loads are mostly reduced by the Path-length modulator (PLM) and by the special wedge-shaped window provided with anti-reflecting grooves on both surfaces to suppress the Fabry-Perot interferences.

Cold load reflectivity

The accuracy of the calibrated atmospheric signal depends strongly on the quality of the reference loads.The reference loads do not radiate as perfect

black bodies and the reflectivity coefficient of the cold load at frequencies around 600 GHz is approximately 0.01 to 0.05 [Kleipool et al., 1999] [8]. Due to reflections, part of the ambient radiation will be reflected into the receiver input and the radiating temperature of the loads will be changed.

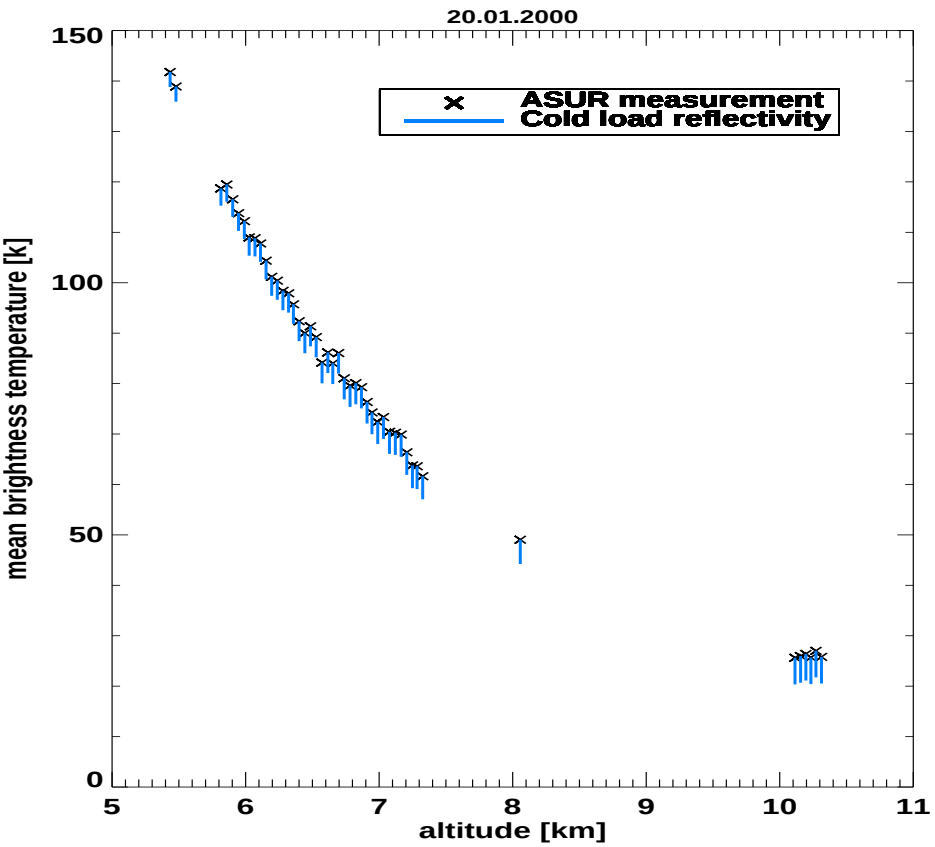

Figure 5.7: The measured brightness temperature by ASUR and the errors respecting to the cold load reflectivity.

For the hot load, which is at ambient temperature no correction is needed since the reflected temperature is equal to the load temperature (both ambient). The observed radiating temperature T'_{atm} can be expressed by

$$T'_{atm} = (1 - R)T_{atm} + RT_h \tag{5.1}$$

The error estimate is given for R=0.02 and $T_h = 290K$.

Pointing accuracy

An uncertainty in the exact zenith angle produces some errors in the measured spectrum. The pointing angle is depending on the roll angle of the

aircraft. Therefore the actual pointing angle is continuously monitored during the measurements and it is adjusted before a single spectrum is observed. The estimated error for the pointing angle is about 0.5 degree.

Figure 5.8 shows the calculated brightness temperatures for the zenith angles 77.5° and 78.5°. As can be seen in the Figure 5.8 the error is about 2.5 % for a deviation 0.5 degree in angle because the path length through the atmosphere changes.

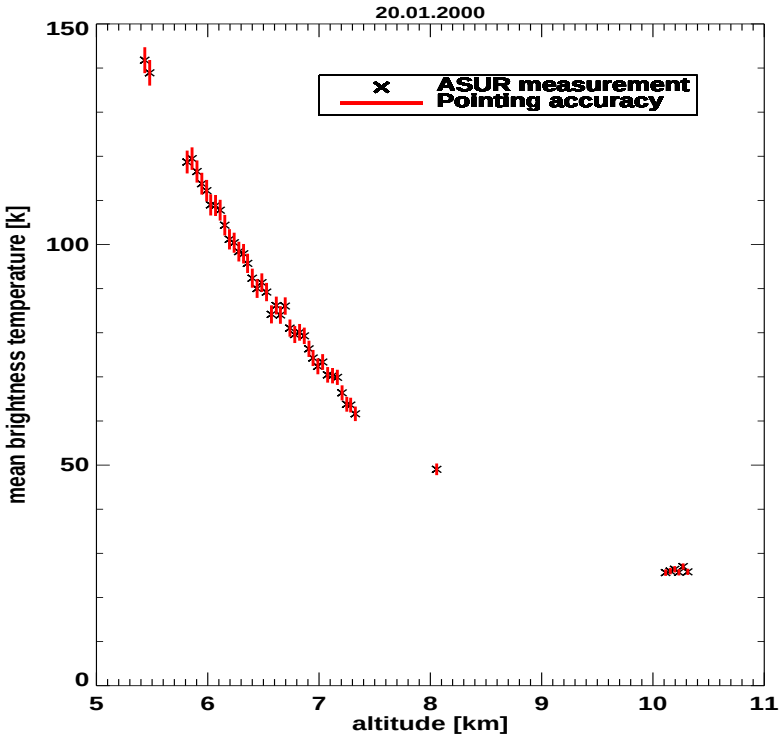

Figure 5.8: The observed brightness temperature by ASUR and the errors for 0.5 degrees change in zenith angle.

The total errors in the measured brightness temperature are listed in Table 5.1.

Error source	Altitude(km)	Error(K)
Measurement noise	5.5 - 10.5	0.9 - 0.6
Pointing error	5.5 - 10.5	2.9 - 0.7
Cold load reflectivity	5.5 - 10.5	3.0 - 5.3
Total error	5.5 - 10.5	4.2 - 5.4

Table 5.1: List of the error sources and errors in the observed brightness temperature by ASUR sensor at different altitudes.

5.2.2 Errors in the calculated brightness temperature

In order to study the sensitivity of the atmospheric parameters as input to the radiative transfer model uncertainties in the volume mixing ratio have been investigated.

Error in the VMR profile of water vapor

The volume mixing ratio profile has an uncertainty, that can be defined for two altitude ranges:

From observed to maximum flight altitude: the water vapor profiles are obtained from in-situ instrument on board the DC-8 aircraft. The Near-Infrared Tunable Diode laser has an accuracy about 5 percent. Hence a calculation with change of 5 percent in the water vapor has been performed and it includes a change of 2 K at low altitudes (5.5 km) and about 0.5 K at high altitudes (10.5 km) (Fig 5.9).

From maximum flight altitude upto 95 km: the water vapor profiles are taken from Chiou (SAGE II) climatological data and a calculation with change about 20 percent in the water vapor profile has been done. As can be seen in Figure 5.9 the change is about 0.4 K at low altitudes and 0.7 K at high altitudes.

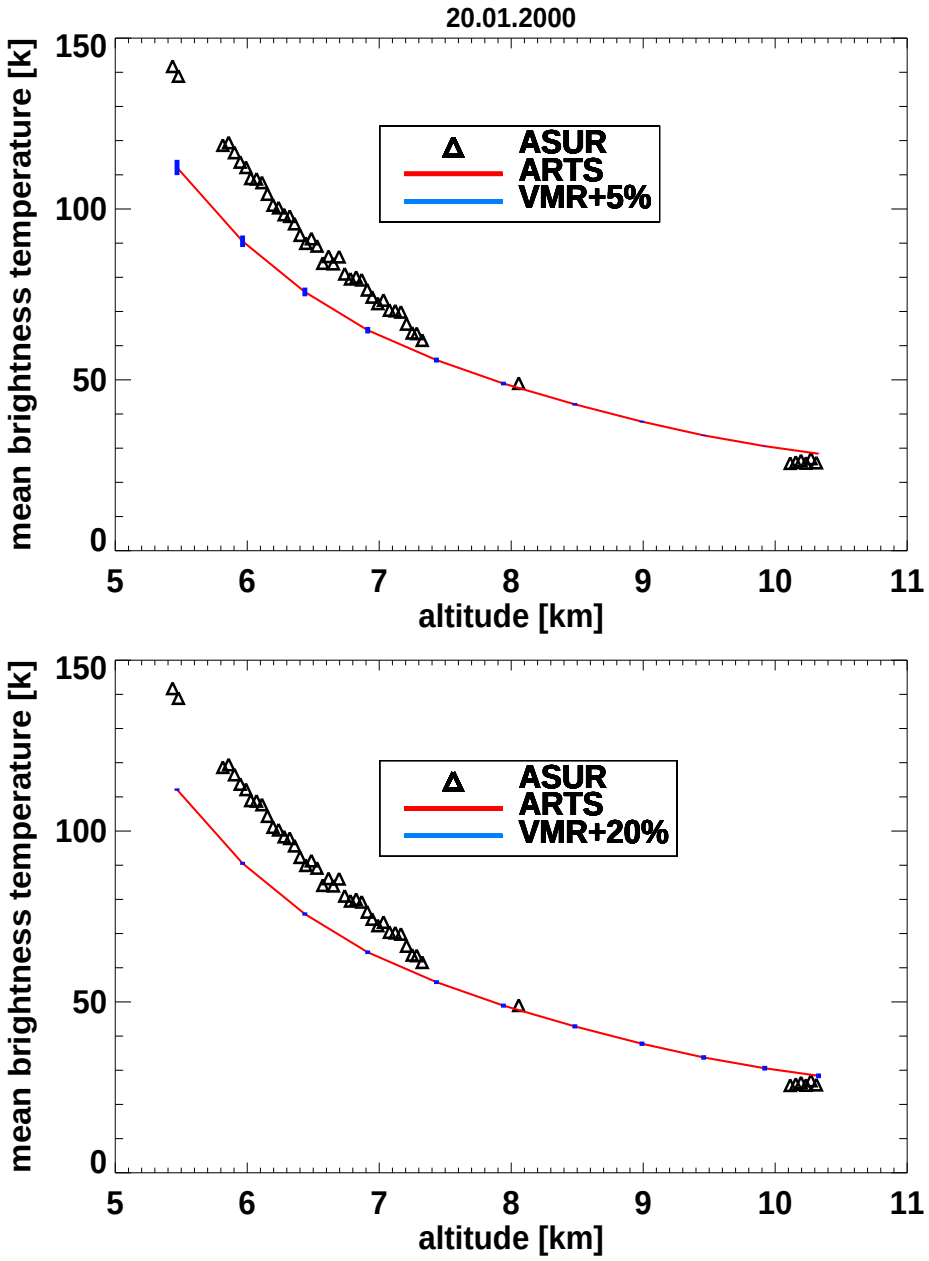

Figure 5.9: The measured brightness temperature, the calculated brightness temperature and errors corresponding to the calculation with a change of 5 percent in volume mixing ratio of water vapor from observed to maximum flight altitude (top) and a change of 20 percent in volume mixing ratio of water vapor from maximum flight altitude up to 95 km (bottom).

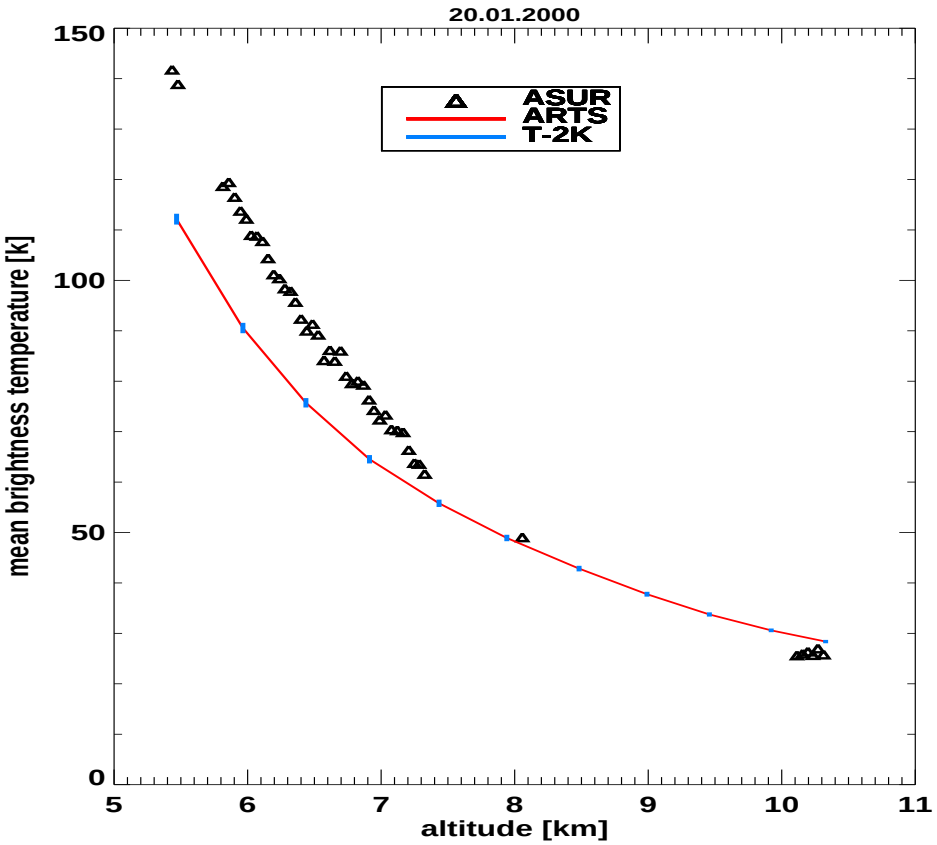

Figure 5.10: The observed brightness temperature by ASUR, the calculated .brightness temperature by ARTS and errors corresponding to the calculation with a change of 2 K in temperature profile from observed flight altitude up to 95 km.

Error in the temperature profile

The meteorological temperature profiles as input to the radiative transfer model have uncertainties that are estimated to be about 2 K. A calculation with a change of 2 K from observed altitude up to 95 km has been performed since the error of the temperature measurements by the DC-8 sensor amounts to 2 K as well.

As can be seen in Figure 5.10 a change about 2 K in the temperature profile includes an error about 1 K at low altitudes (5.5 km) and 0.3 K at high altitudes (10.5 km).

Error in the HCl and O_3 lines

Error source	Altitude(km)	Error(K)
Volume mixing ratio (% 20)	5.5 - 10.5	2.2 - 0.7
Volume mixing ratio (% 5)	5.5 - 10.5	0.4 - 0.7
Temperature	5.5 - 10.5	1.1 - 0.3
HCl and O_3 lines	5.5 - 10.5	0.3 - 0.6
Total error	5.5 - 10.5	2.5 - 0.9

Table 5.2: List of the most error sources in the calculated brightness temperature at different altitudes.

To study the influence in the HCl and O_3 lines, the errors can be determined in two altitude ranges:

From observed to maximum flight altitude: the volume mixing ratio profiles are taken from FASCOD climatological data. For clear air the arctic an estimated deviation from climatology profile by 50 percent has been considered and it includes very small uncertainty about 0.03 K at low altitudes and 0.003 K at high altitudes.

From maximum flight altitude upto 95 km: the volume mixing ratios are obtained from ASUR data with 15 percent accuracy [von koenig] [13]. At low altitudes the uncertainty is about 0.3 K and at high altitudes about 0.6 K.

The summarized errors in the calculated brightness temperature are given in Table 5.2.

5.3 Conclusions

The comparison between the observed brightness temperature by the ASUR sensor and the calculated brightness temperature by the forward model ARTS with consideration of the most important error sources in the observations and calculations are shown in Figure 5.11.

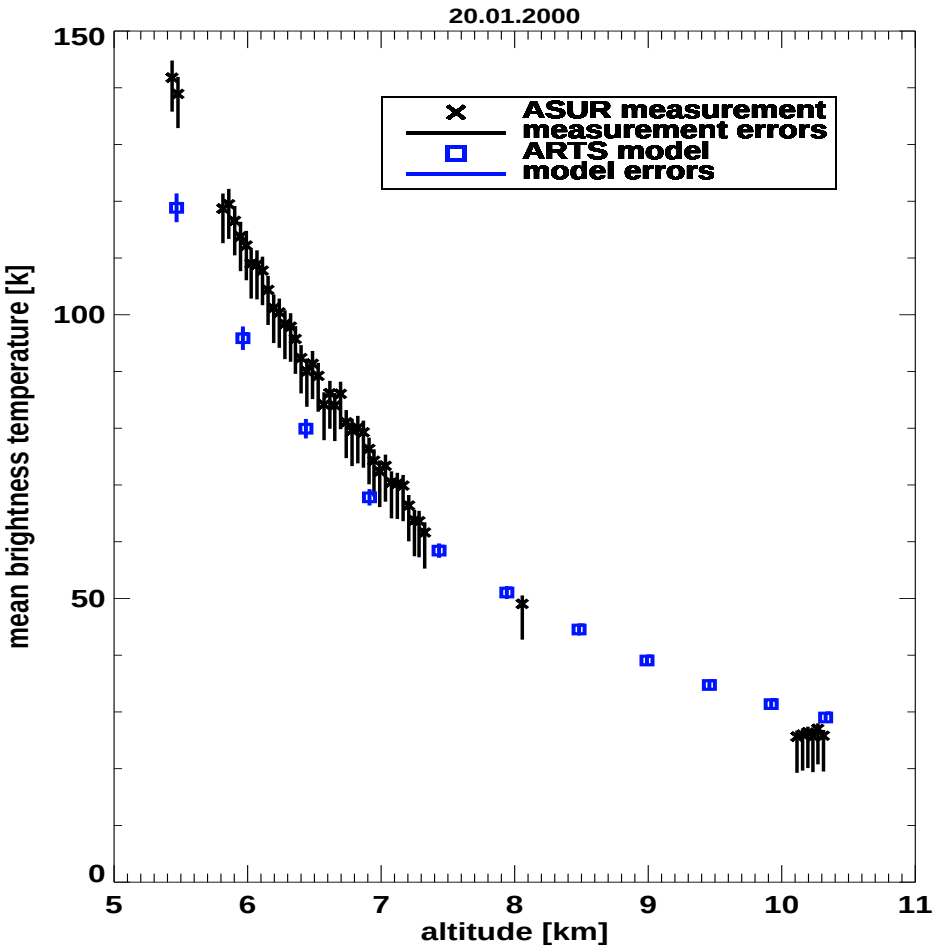

Figure 5.11: The brightness temperatures measured by ASUR in up-looking mode on January 20 th, 2000 are compared with calculations by the radiative transfer model ARTS considering the errors in the measurements and model.

As can be seen in this figure the measured brightness temperature by the ASUR sensor is in good agreement with the theoretical calculation by ARTS in the altitude range between 7 and 10 km. Below 7 km the difference between observations and calculation increases down to the lowest altitude of

5.5 km, where the water vapor density is high. At these altitudes the model predicts insufficient absorption.

The corresponding observation and calculation uncertainties are larger at low altitudes.

However, at low altitudes there are also differences between the three empirical water vapor continuum models (Liebe 89, Liebe 93 and Rosenkranz 98) and the Liebe 93 model gives here the slightly better approach (from Figure 5.4).

Summary

Aircraft measurements at 626 GHz with the submillimeter radiometer ASUR on board the NASA research aircraft DC-8 in the winter 1999/2000 during the THESEO/SOLVE campaign were used for continuum analysis.

In addition, observations of water vapor absorption from an in-situ instrument on board the DC-8 were used for radiation forward calculations.

The measured and the calculated brightness temperatures are compared in terms of three water vapor continuum models (Liebe 89, Liebe 93 and Rosenkranz) and one nitrogen continuum model (Liebe 93).

In general, below 9 km all models tend to under predict the brightness temperature and above 9 km over predict the brightness temperature. The agreement is generally better at altitudes between 7 and 10 km.

From three water vapor continuum models Liebe 93 model shows slightly better approach to the measurements.

ASUR measurements during the descent of the aircraft have been compared with calculations by the radiative transfer model ARTS during three flights, namely on January 20 th, 2000, on March 5 th, 2000 and on March 13 th, 2000 and the results were discussed.

The contribution of water vapor continuum and nitrogen continuum to the total absorption at the upper troposphere and lower stratosphere was investigated.

Results from one flight were presented including a detailed error analysis. The error analysis takes into account most important errors and uncertainties and provides an estimate of errors in the observations and calculations.

Acknowledgements

First of all, I would like to thank Armin Kleinböhl for his collaboration without whom this work would not have been possible. I would like to thank my supervisor Dr. Harry Küllmann and my colleagues Jayanarayanan for useful comments on the manuscript and valuable help and Dr. Holger Bremer of my own group. I have to thank Dr. Miriam von König for the helpful discussion and comments. I want to thank Thomas Kuhn and Viju Oommen John from the SAT research group for helpful advise and discussion on the radiative transfer model ARTS. I want to express my gratitude to prof. K.Künzi and the PEP team led by Prof. Bleck-Neuhaus for giving me not only support but also the possibility for my studies.

Bibliography

[1] H. Bremer. *Messung von dynamischen Tracern und Ozone in der arktischen stratospheare.* PhD thesis, Universitat Bremen, 2001.

[2] S. Buehler. *Microwave Limb Sounding of the Stratosphere and Upper Troposhere.* PhD thesis, Universitaet Bremen, 1999.

[3] S. Buehler and P. Eriksson, editors. *Atmospheric Millimeter and Sub-Millimeter Wave Radiative Transfer Modeling.* Berichte aus der Physik. Shaker Verlag, Aachen, 2000.

[4] S. Buehler, P. Eriksson, W. Haas, N. Koulev, T. K uhn, and O. Lemke. *ARTS User Guide.* http://www.sat.uni-bremen.de/arts, 2002.

[5] S. Crewell. *Submillimeter-Radiometrie mit einem flugzeuggetragenen Empfaenger zur Messung atmosphaerischer Spurenstoffe.* PhD thesis, Universitaet Bremen, 1993.

[6] P. Eriksson. *Microwave Radiometric Observations of the Middle Atmosphere: Simulations and Inversions.* PhD thesis, Chalmers University of Technology, Goeteborg, 1999.

[7] A. Kleinboehl, H. Bremer, M. von Koenig, H. Kuellmann, K. Kuenzi, A. P. H. Goede, E. Browell, W. B. Grant, G. C. Toon, T. Blumenstock, B. Galle, B.-M. Sinnhuber, and M. Chipperfield. Vortexwide denitrification of the arctic polar stratosphere in winter 1999/2000 determined by remote observations. *J.Geophys.Res. 108,D5,8305, 10,1029/2001 JD 001042, 2003*, 2001. accepted.

[8] Q. L. Kleipool, F. Hellmich, A. P. H. Goede, H. Schrijver, M. van den Broek, K. Kuenzi, H. Kuellmann, H. Bremer, M. von Koenig, and H. Hetzheim. Measurements of clo and hcl profiles during the arctic winter of 1999 with consequences for ozone depletion. In *Proceedings Fifth European Symposium on Stratospheric Ozone*, number Air pollution research report 73, pages 276–279, St. Jean de Luz, France, 1999.

[9] H. J. Liebe, G. A. Hufford, and M. G. Cotton. Propagation modeling of moist air and suspended water/ice particles at frequencies below 1000 ghz. In *52nd Specialists' Meeting of the Electromagnetic Wave Propagation Panel*, Palma de Mallorca, Spain, 1993.

[10] Tipping RH Ma Q. Water vapor continuum in the millimeter spectral region. *Journal of Chemical Physics*, 93:6127–6139, 1990.

[11] P.W. Rosenkranz. Absorption of microwaves by atmospheric gases. In *Atmospheric Remote Sensing by Microwave Radiometry, edited byM.A. Janssen*, pages 37–90, 1993.

[12] P.W. Rosenkranz. Water-Vapour Microwave Continuum Absorption: A Comparison of Measurements and Models. *Radio Sci.*, 33:919–928, 1998.

[13] M. von Koenig. *Chloraktivierung und PSC-Bildung in der arktichen Stratosphare: Analyse und Interpretation flugzeuggetragenen Submillimeterwellenmessungen.* PhD thesis, Universitat Bremen, 2001.